**Doctoral Thesis**

# The effect of electric field and temperature on the structural order of water molecules around biomedical materials between nano metal plates by molecular dynamics simulations

**by**

**Le Nhu Minh Tue**

**January 2023**

**Graduate School of Simulation Studies**
**University of Hyogo**

Le Nhu Minh Tue's Ph.D. Thesis

is approved by

| | | |
|---|---|---|
| Committee member | Prof. Hitoshi Washizu | _____ |
| Committee member | Prof. Yutaka Hata | _____ |
| Committee member | Prof. Shugo Yasuda | _____ |
| Committee member | Prof. Hiraku Oshima | _____ |

January, 2022

# List of Publications

1. Structural order of water molecules around polyrotaxane including PEG, α-cyclodextrin, and α-lipoic acid linker on gold surface by molecular dynamics simulations
   Physical Chemistry Chemical Physics
   2022 | Journal article
   DOI: 10.1039/D1CP04487G
   CONTRIBUTORS: **Tue Minh Nhu Le**; Le Van Sang; Hitoshi Washizu

2. The effect of electric field on the structural order of water molecules around chitosan between nano gold plates determined by molecular dynamics simulations
   Physical Chemistry Chemical Physics
   2022 | Journal article
   DOI: 10.1039/D2CP03916H
   CONTRIBUTORS: **Tue Minh Nhu Le**; Hitoshi Washizu

# CONTENTS

**ABSTRACT**

Water is one of the most important solvents due to its large compound on earth. Water is essential for many chemical reactions, the fluids of all known living organisms, and the main component of biological systems. However, the structure of the molecular water ensemble in the vicinity of the polymers is under discussion. During the past few decades, many experimental and theoretical studies have investigated the hydrated polymer to clarify its structure, especially polymers' bio/blood compatibility. The interactions between water and polymers are dependent on structure, polarity, hydrophilicity or hydrophobicity, and functional groups. In this study, we use the molecular dynamics method to analyze the structure of water in the vicinity of bioactive polymers onto gold surface at various temperatures. The different amounts of TIP3P/B water and external electric field are also considered. Water distributions around functional groups, hydrogen bond network, and tetrahedral order are analyzed to classify various types of water around the polymer. We discovered a tight association between water's tetrahedral arrangement and its XES experiment. We found that four water zones are separating from one another in the range of 1 to 6 Å around polymers. As a result of interactions between water molecules and functional groups like hydroxyl, ether, and ester, intermediate and non-freezing water is generated.

**ACKNOWLEDGEMENTS**

First and foremost, I would like to express my gratitude to professor Hitoshi Washizu, for giving me an opportunity to study here University of Hyogo. I would also like to extend my appreciation to the committee members, Prof. Yutaka Hata, Prof. Shugo Yasuda and Prof. Hiraku Oshima for their valuable comments and suggestions on my Ph.D. thesis and final presentation.

The second, I would also like to thank Dr. Le Van Sang, for introducing me to University of Hyogo, his advice and assistance in keeping my progress on schedule. My grateful thanks are also extended to my fellow graduate students, Islam Rubaiyat and Mitsuyoshi Yagyu for their support me in research work and adjusting my life in Japan.

Finally, I wish to thank my parents for their support and encouragement throughout my study.

"Life is either a daring adventure, or nothing."

Helen Keller

Le Nhu Minh Tue
*University of Hyogo*
*Japan*

*January, 2023*

# 1. Introduction

## 1.1 Water Introduction

Recognizing that liquid water possesses certain peculiar and significant physical and chemical characteristics. In essence, according to scientists, it serves as the background against which the molecular building blocks of life are arranged due to its potency as a solvent, its capacity to form hydrogen bonds, and its amphoteric properties. For instance, simulating biomolecules on computers when they are in a vacuum used to be a frequent technique. This was due in part to the computational difficulty of modelling a polymer chain without taking solvent molecules into account, but it also represented the widespread belief that water just tempers or moderates the fundamental physicochemical interactions that underlie molecular biology. Therefore, water was the matrix of the world and of all its creatures.[1,2]

One water molecule includes of one negatively polarized oxygen atom and two positively polarized hydrogen atoms with different electronegativity (Fig. 1.1). If there are many water molecules present in a system, the polarized nature of the water molecule can be a driving force for an intermolecular interaction known as a hydrogen bond. A hydrogen bond, as defined by the International Union of Pure and Applied Chemistry (IUPAC), is an attractive interaction between an acceptor atom or group such as X-H group in which X is more electronegative than H.[3, 4] The oxygen atom of a water molecule is covered by two non-bonding electron pairs, as can be seen in the structural formulas in Fig. 1.1. While hydrogen atoms are naturally hydrogen bond donor sites, these lone pairs can serve as good acceptor sites for hydrogen bonds.

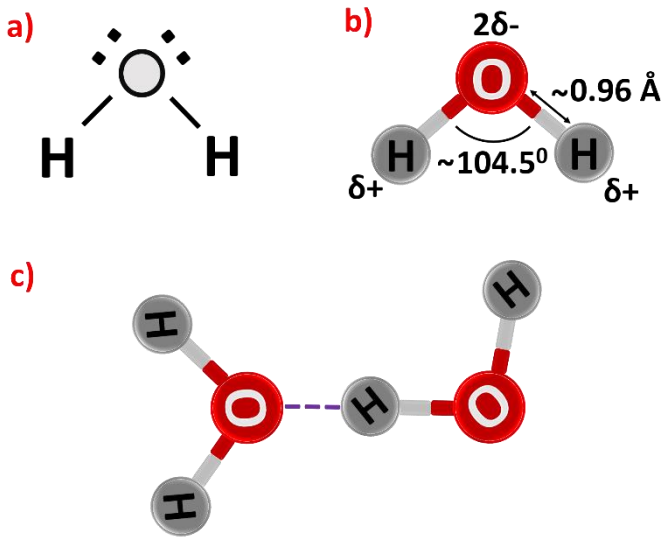


**Fig. 1.1** Formation of a water molecule. **a**) Structural formula. **b**) Schematic model with bond length, angle and electrostatic potential. **c**) Hydrogen bond between two water molecules (purple dashed line)

As a result, "O−H···O " is used to denote the hydrogen bonding between water molecules (Fig. 1.1c). An average hydrogen bond has an enthalpy of a few tens kJ/mol (a few thousand cm-1).[5-7] Such a number can change the entire characteristics of water and is greater than a van der Waals interaction. For instance, hydrogen bonding explains the resistance to evaporation when heated. Due to this, water has a higher boiling point than would be predicted solely on its molecular weight. It is now beyond dispute that the hydrogen bond controls water's distinctive properties.

### 1.2 Hydrated polymer and biomedical materials

In medical applications, biomedical materials are utilized to repair or replace damaged tissue and to control biological functions based on biophysical and biochemical cues.[8,9] The fabrication of biomedical materials necessitates interdisciplinary understanding of material science and technology, basic biological processes, and interactions between materials and living things. Surface features of biomedical materials have an inescapable impact on their molecular biological characteristics and biomedical applications because they influence biological processes such as biological signaling, transportation, and kinetics.[10,11]

Since the biomedical materials, including biological fluids, are used in water, the hydration of biomedical material will appear on the surfaces. Interfacial water is defined as the water at the interface between water and the surface of the material. Interfacial water interacts with the surface

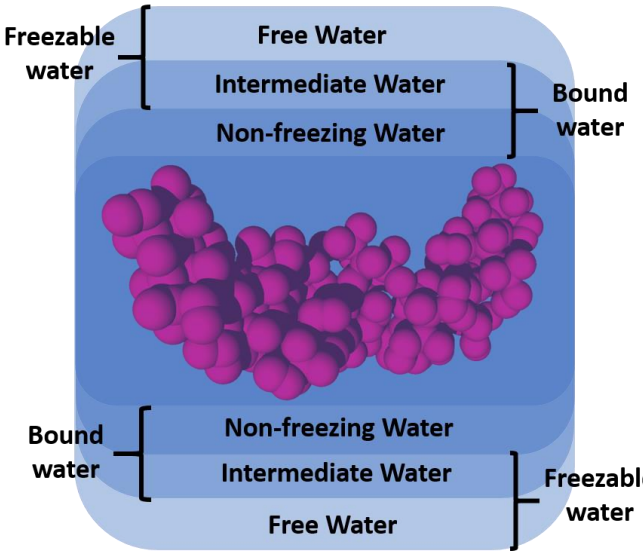


**Fig. 1.2** The classification of interfacial water was divided into three categories around a material in this regard: free water (FW), intermediate water (IW), and non-freezing water (NFW)

through hydrogen bonding, hydrophobic hydration, van der Waals contacts, and electrostatic interactions.[12,13] The network of water molecules is reformed by the interaction with materials at the interface, despite the fact that in bulk water, water molecules dynamically form a cluster network that does not interact with materials. A distinctive hydration structure is created as a result of the restructuring of water molecules at the interface.

Due to changes in measuring techniques and the definition of interfacial water states, the classification of interfacial water is varied and intricate. On the basis of their thermal behavior and mechanism of binding, the interfacial water was divided into three categories in this regard: free water (FW), intermediate water (IW), and non-freezing water (NFW).[14,15] Since the non-freezing water is not frozen below 273 K and lacks any structures, it is regarded as disorder. The intermediate water, on the other hand, has a tetrahedral structure when the temperature decreases to below temperature 273 K, making it the order. The free water at temperature 273 K is regarded as the order since it has an ice structure. Free water, furthermore, is regarded as bulk water when temperature is higher than 273 K and has no interaction with any polymers.

At the room temperature, because the intermediate water is weakly (loosely) attached to the surface of biomedical materials such as polymer molecules, it forms a more stable structure than free water, while non-freezing water (tightly bound water) has significant interactions with polymer molecules. The direct contact between the protein or cell and the polymer surface, which is necessary for biocompatibility, is therefore prevented if the intervening water layer grows thick enough.[15] Breaking the

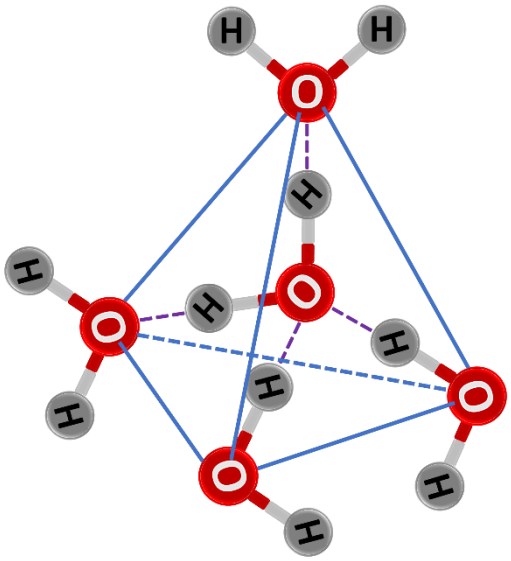


**Fig. 1.3** Schematic model of the 4-coordinated water molecule

intermolecular hydrogen bond between water molecules causes loosely bound water to develop, which is subsequently linked near to the hydroxyl groups of polymers to create a layer.[16] Accordingly, the water layer can be categorized as firmly bound, closely bound, or free based on how near or how far away it is from the polymer. In the processes of protein adsorption, platelet adhesion, adhesive cell adhesion, proliferation, and differentiation, the amount of interfacial water present on the surfaces of biomedical materials is essential. As a consequence, the interfacial water of biomedical materials plays an important role in the design of advanced biomedical materials. However, the formations of these 3 types of water are still debated until now. The studies in chapter 2 and 3 contribute to clarify these issues.

Nowadays, due to the rapid development of nanotechnology, nanomaterials are used in various applications, especially for biomedical materials in health and medicine. Nanomaterials, especially gold, have a wide range of chemical, optical, and physical properties that make them especially interesting for biomedical applications such as drug delivery. Gold nanostructures are also used in enhancing scientific analytical instruments such as photoluminescence, localized surface plasmon resonance, resistance, surface-enhanced Raman scattering, bioinert nature or photo thermal effect.[17-20] With the new properties of nanomaterials, the associations by various nanomaterials in one composite material are necessary for developing in materials science in the future. Therefore, these studies in this thesis combine gold and polymers as the constituent materials to survey the interfacial water of biomedical materials.

## 1.3 The relationship between tetrahedral order method and XES experiment

In principle, up to four hydrogen bonds can be formed around a single $H_2O$ molecule due to the fact that it has two hydrogen bond acceptor sites (two lone pairs) and donor sites (two OH groups) (Fig. 1.3 and Fig. 1.1). In practice, the local structure of liquid water is united with the propensity of water molecules to make four hydrogen bonds with their closest neighbors in a tetrahedral arrangement. As a result, the liquid state structure is comprised of a fluctuation, open network with local tetrahedral order. However, this tetrahedral order increases when the temperature decreases below 273 K and tetragonal phase of water changes from liquid to solid state with structures such as ice Ic and Ih. In the case of applying an electric field,

tetragonal phase, derived from ice Ic, has a cubic diamond-type oxygen sublattice structure.[21,22] These network creation and structure are the result of the numerous hydrogen bond formation. Structures and dynamics of hydrogen-bonded water networks have drawn a lot of attention because of the hydrogen bond's inherent significance in the study of water.

Measuring structural order in liquids and glasses has proven particularly complicated in molecular dynamics simulation because, while such systems have short-range order, they lack long-range crystalline organization. However, it is still challenging to accurately describe fluids like water, where directional attractions (hydrogen bonds) combine with short-range repulsions to determine the relative orientation of neighboring molecules as well as their instantaneous separation. While some improvement has been made using model systems of hard spheres, this challenge still exists.[23,24] This challenge is specifically significant when considering the unusual thermodynamic and kinetic properties of water, which have long been qualitatively explained in terms of underlying structural factors. Jeffrey R. Errington & Pablo G. Debenedetti[25] aim to get a superior comprehension of these structure-property interactions by investigating orientational order parameter q for 4-coordinated water molecules in a water model.[26,27] A convenient measurement of the local tetrahedral associated with a given oxygen atom i is given by:

$$q_{tet} = 1 - \frac{3}{8}\sum_{j=1}^{3}\sum_{k=j+1}^{4}\left(\cos\theta_{ijk} + \frac{1}{3}\right)^2 \quad (1)$$

where θ is the angle between the bond vectors $r_{ij}$ and $r_{ik}$, j and k labels are typical for the four nearest oxygen atoms. The value of q can range from 0 to 1, where 0 is for the ideal gas, and 1 is for perfect tetrahedral structures.

This tetrahedral order value also matches the results of the water X-ray emission spectroscopy (XES) experiment. One of the direct observational techniques frequently used to study the electronic transitions between core and valence orbitals in the spectroscopy of liquid water is XES.[28] Previous investigations showed that the sharp $1b_1$' and $1b_1$'' peaks in the high-resolution O 1s XES spectra of liquid water are separated by the non-bonding $1b_1$ lone-pair.[29] Due to the presence of a four-fold H-bonded structure ($1b_1$') and lower ones, these two peaks can be linked to two different structural geometries in liquid water ($1b_1$''). These two peaks $1b_1$' and $1b_1$'' were found to change from the ice to gas phase based on practical and theoretical studies of excitation energy-dependent spectra at various

temperatures.

## Reference


1. Szent-Gyo¨rgyi, A. In *Cell-Associated Water*; Drost-Hansen, W, Clegg, J. S., Eds.; Academic Press: New York, 1979
2. Jacobi, J., Ed. *Paracelsus: Selected Writings*; Princeton University Press, 1979; p 13
3. E. Arunan, G.R. Desiraju, R.A. Klein, J. Sadlej, S. Scheiner, I. Alkorta, D.C. Clary, R.H. Crabtree, J.J. Dannenberg, P. Hobza, H.G. Kjaergaard, A.C. Legon, B. Mennucci, D.J. Nesbitt, Pure Appl. Chem. 83, 1637–1641 (2011)
4. E. Arunan, G.R. Desiraju, R.A. Klein, J. Sadlej, S. Scheiner, I. Alkorta, D.C. Clary, R.H. Crabtree, J.J. Dannenberg, P. Hobza, H.G. Kjaergaard, A.C. Legon, B. Mennucci, D.J. Nesbitt, Pure Appl. Chem. 83, 1619–1636 (2011)
5. J.N. Israelachvili, Intermolecular and Surface Forces, 2nd edn. (Academic Press, London, 1992)
6. L. Pauling, The Nature of the Chemical Bond, 3rd edn. (Cornell University Press, New York, 1960)
7. P.W. Atkins, Physical Chemistry, 6th edn. (Oxford University Press, Oxford, 1998)
8. D. Shan, E. Gerhard, C. Zhang, J.W. Tierney, D. Xie, Z. Liu, J. Yang, Bioact. Mater. 3 (4) (2018) 434–445
9. M.T. Chorsi, E.J. Curry, H.T. Chorsi, R. Das, J. Baroody, P.K. Purohit, H. Ilies, T.D. Nguyen, Adv. Mater. 31(1) (2019) 1802084
10. J.J. Rice, M.M. Martino, L. De Laporte, F. Tortelli, P.S. Briquez, J.A. Hubbell, Adv. Healthc. Mater. 2 (1) (2013) 57–71
11. P. Wang, C. Wang, L. Lu, X. Li, W. Wang, M. Zhao, L. Hu, A.M. El-Toni, Q. Li, F. Zhang, Biomaterials. 141 (2017) 223–232
12. C. Sendner, D. Horinek, L. Bocquet, R.R. Netz, Langmuir. 25 (18) (2009) 10768–10781
13. M.P. Goertz, J.E. Houston, X.-Y. Zhu, Langmuir. 23 (10) (2007) 5491–5497
14. M. Tanaka, K. Sato, E. Kitakami, S. Kobayashi, T. Hoshiba, K. Fukushima, Polym. J. 47 (2) (2015) 114–121
15. M. Tanaka, T. Hayashi, S. Morita, Polym. J. 45 (7) (2013) 701–710
16. K. Nakamura, T. Hatakeyama and H. Hatakeyama, Polymer. 1983, 24, 871–876
17. Nelson BC, Petersen EJ, Marquis BJ, et al., Nanotoxicology. 2013, 7(1), 21–29.
18. Silva CO, Rijo P, Molpeceres J, et al., Ther Deliv. 2016, 7(5), 287–304.
19. Rau LR, Huang WY, Liaw JW, et al., Int J Nanomedicine. 2016, 11, 3461–3473.
20. Yang X, Yang M, Pang B, et al., Chem Rev. 2015, 115(19), 10410–10488.

21. Q. Zhu, A. R. Oganov, C. W. Glass and H. T. Stokes, Acta Crystallographica Section B, 2012, 68, 215-226
22. A. T. Celebi, M. Barisik and A. Beskok, The Journal of Chemical Physics, 2017, 147, 164311
23. Torquato, S., Truskett, T. M. & Debenedetti, P. G., Phys. Rev. Lett. 84, 2064–2067 (2000)
24. Truskett, T. M., Torquato, S. & Debenedetti, P. G., Phys. Rev. E 62, 993–1001 (2000)
25. J. R. Errington and P. G. Debenedetti, Nature, 2001, 409, 318–321
26. Chau, P.-L. & Hardwick, A. J. A, Mol. Phys. 93, 511–518 (1998)
27. Berendsen, H. J. C., Grigera, R. J. & Stroatsma, T. P., J. Phys. Chem. 91, 6269–6271 (1987)
28. E. Gilberg, M. J. Hanus and B. Foltz, J. Chem. Phys., 1982, 76, 5093–5097
29. T. Tokushima, Y. Harada, O. Takahashi, Y. Senba, H. Ohashi, L. G. M. Pettersson, A. Nilsson and S. Shin, Chem. Phys. Lett., 2008, 460, 387–400

## 2. The effect of temperatures on the structural order of water molecules around polyrotaxane

### 2.1 Abstract

In materials science, water plays an important part, especially at the molecular level. It shows various properties when sorbed onto surfaces of polymers. The structure of the molecular water ensemble in the vicinity of the polymers is under discussion. In this study, we used molecular dynamics methods to analyze the structure of water in the vicinity of the polymer polyrotaxane (PR), composed of α-cyclodextrins (α-CDs), a poly(ethylene glycol) (PEG) axial chain, and α-lipoic acid linkers, at various temperatures. The distribution of water around the functional groups, hydrogen bond network, and tetrahedral order were analyzed to classify the various types of water around the polymer. We found that the tetrahedral order of water had a strained relationship from the XES experiment. Four water regions were separated from each other in the vicinity of 1 to 5 Å around PR. The intermediate and nonfreezing water were formed due to the interaction between water molecules and the functional groups, such as hydroxyl, ether, and ester.

### 2.2 Introduction

Water is an essential solvent due to it being the most common compound on Earth. Water is necessary for many chemical reactions, is the fluid of all known living organisms, and is the main component of biological systems and materials science. Many extraordinary properties of water often originate from the presence of hydrogen bonds. Although the science of bulk water and water on hydrophobic surfaces is well understood, comprehension of the hydrophilic surface still needs extensive study, especially for superhydrophilic materials. In a water molecule, the oxygen atom makes a 104.51 angle with the hydrogen atoms.[1] Because of its polarity, water can dissolve hydrophilic proteins, ions, gases, and organic liquids.[2] One water molecule in the liquid or solid phase usually has four hydrogen bonds with its neighboring molecules. The hydrogen atoms are close to two corners of a tetrahedron centered on the oxygen atom.[3]

In contrast, the other two corners are lone pairs of valence electrons that the oxygen atom uses to pair up with two hydrogen atoms of different water molecules. In a perfect tetrahedron, the atoms form a 109.51 angle, but the lone pair repulsion is greater than the repulsion between the hydrogen

atoms.[4] Therefore, water has many applications at the nanoscale, especially in biomaterials.[5,6] During the past few decades, many experimental and theoretical studies have investigated the hydrated polymer to clarify its structure, especially polymer bio/blood compatibility.[7,8] The interactions between water and polymers are dependent on structure, polarity, hydrophilicity or hydrophobicity, and functional groups.[9–12] The reordering of water molecules under the influence of the above causes has resulted in the formation of various geometries of water, such as tetrahedral order and different constituted conformations or layering around polymers.[13–15] Several chemical and physical experimental methods have been used to identify and quantify the different types of water in the regions close to the interfaces. The three primary techniques used are differential scanning calorimetry (DSC), nuclear magnetic resonance (NMR), and infrared (IR) spectroscopy.[16–19] The water around a polymer is classified into three types:

- Free water (or freezing water)
- Freezing-bound water (or intermediate water)
- Non-freezing water (or non-freezing-bound water)

The water layer formed from intermediate water is a more stable structure than free water due to it being weakly (loosely) bound to the polymer molecule, while non-freezing water (tightly bound water) has strong interactions with polymer molecules. Thus, if the intermediate water layer becomes sufficiently thick, it prevents the protein or cell from directly contacting the polymer surface, which is essential for biocompatibility.[20] Loosely bound water arises by breaking the intermolecular hydrogen bonding between water molecules, and these water molecules are then attached close to the hydroxyl groups of polymers to form a layer.[21] Therefore, the water layer can be classified as tightly bound, closely bound, or free depending on the distance between it and the polymer.

This study examined the types of water by simulation methods and classified water by its tetrahedral order and density in regions around the polymer placed on a gold surface. The simulation results were related to those reported in previous experimental and theoretical studies. Gold has been studied as a functionalized material in recent decades due to the various applications of gold nanoparticles in biological systems, especially studies on wetting water droplets on gold surfaces with the occurrence of polymers.[22,23] Gold is also commonly seen in applications such as nanofluidic manipulation, lab on a chip, and electrowetting.[24,25] In this work,

in addition to investigations for water, we also studied the molecular dynamics properties of polyrotaxane (PR),[26–29] composed of α-cyclodextrins (α-CDs) with α-lipoic acid (ALA) linkers and a polyethylene glycol (PEG) axial chain, placed on a gold surface. PEG is a polymer with the subunit C–O–C and is soluble in water, except for PEG with high molecular weight.[30–32] Thus, it is a prominent solvent for low-temperature crystallography, modulators of osmotic pressure, and polymer–drug carriers in drug delivery.[33–37]

Furthermore, each α-CD in PR has 18 hydroxyl groups which contribute to the formation of intermediate water layers. In this study, we chose the water model TIP3P/B because it is appropriate for the explicit calculation of long-range electrostatic interactions. In addition, this water model can obtain the improved representation of long-range structures for a more tetrahedral HOH angle. Therefore, TIP3P/B is very important for the categorization of the type of water through tetrahedral order calculation.[38]

We evaluated the water structure based on the ordering situation at its different contents, corresponding to the X-ray emission spectroscopy (XES) experiment for water. XES is one of the direct observational methods commonly applied to investigating the spectroscopy of liquid water involving electronic transitions between core and valence orbitals.[39] Previous studies demonstrated that the non-bonding $1b_1$ lone-pair separates two sharp peaks $1b_1'$ and $1b_1''$ in the high-resolution O 1s XES spectra of liquid water.[40] These two peaks can be related to two distinct structural geometries in liquid water due to the existence of a four-fold H-bonded structure ($1b_1'$) and lower ones ($1b_1''$). From experimental and theoretical observations of excitation energy-dependent spectra at various temperatures, $1b_1'$ and $1b_1''$ were found to vary from the ice to gas phase.

### 2.3 Results and discussion

#### Water classification

Fig. 2.1b and a show the chemical structure of α-CD with the ALA linker and the configuration of PR, including PEG, α-CDs, and ALA linkers, respectively. Fig. 2.1c presents the snapshots of the initial and final corresponding configurations of the three investigated systems (WL, WN, and WH) based on the numbers of TIP3P/B water molecules of 4900, 9025, and 18225, respectively. In each system, PR and water molecules are inserted between two gold plates (100) perpendicular to the z-direction. By

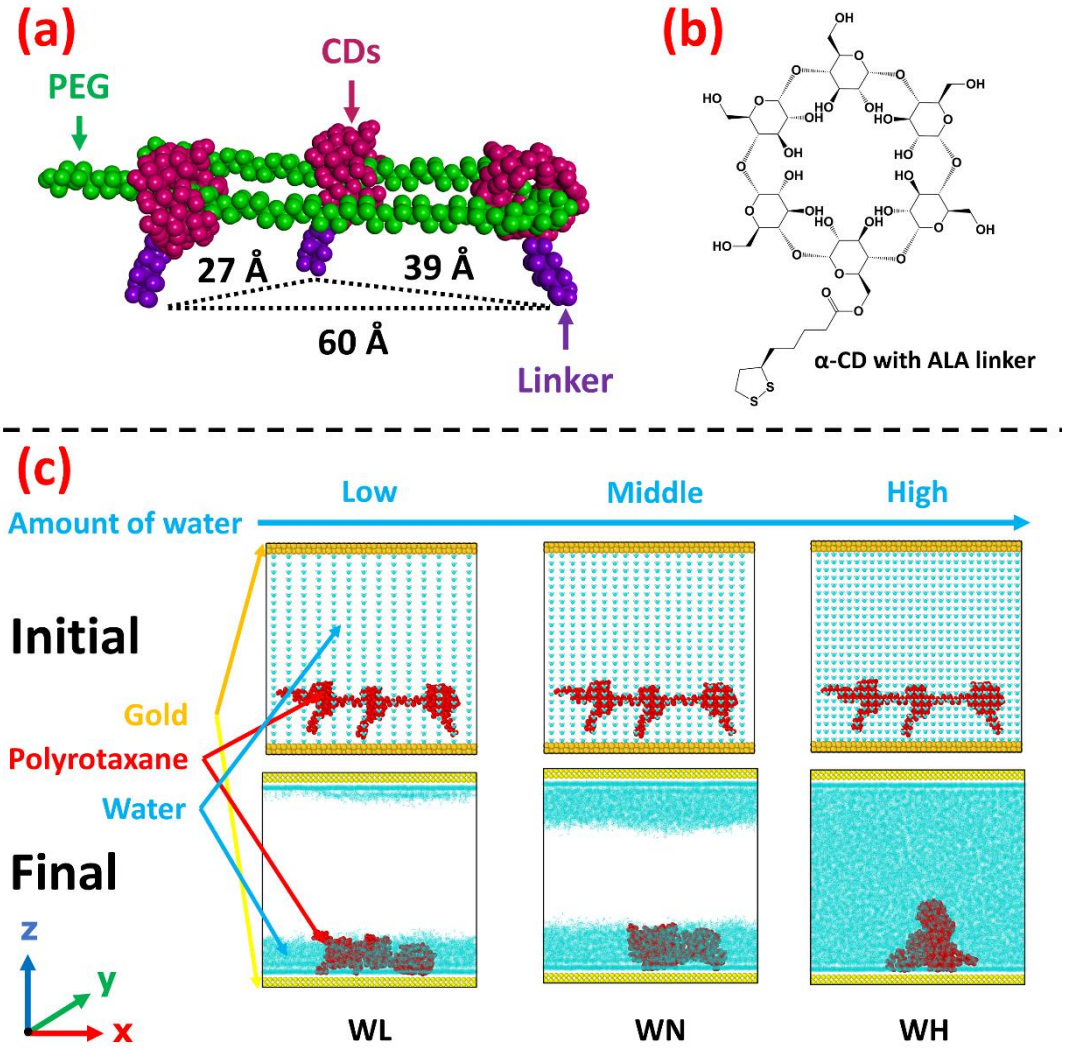


**Figure 2.1.** (a) Configuration of PR; (b) Chemical structure of α-CD with ALA linker; (c) Initial Models and Final Models after running simulation at temperatures 300 K and 250 K with different amount of water – WL, WN, and WH.

monitoring the physical properties of water at the temperatures of 250 and 300 K, for simplicity, the WH systems are named as 25WH and 30WH, respectively (similarly for the other systems: 25WN, 30WN, 25WL, and 30WL). We also examined the properties of WH at temperatures of 250 and 300 K by removing gold and the polymer (named 25PW and 30PW) or removing the polymer (named 25WG and 30WG). The gold plates are fixed during the simulations, and the periodic boundary conditions are applied along the x- and y-directions. The details of the systems and the simulations are described in the Simulation section and Table 2.S2 (ESI†).

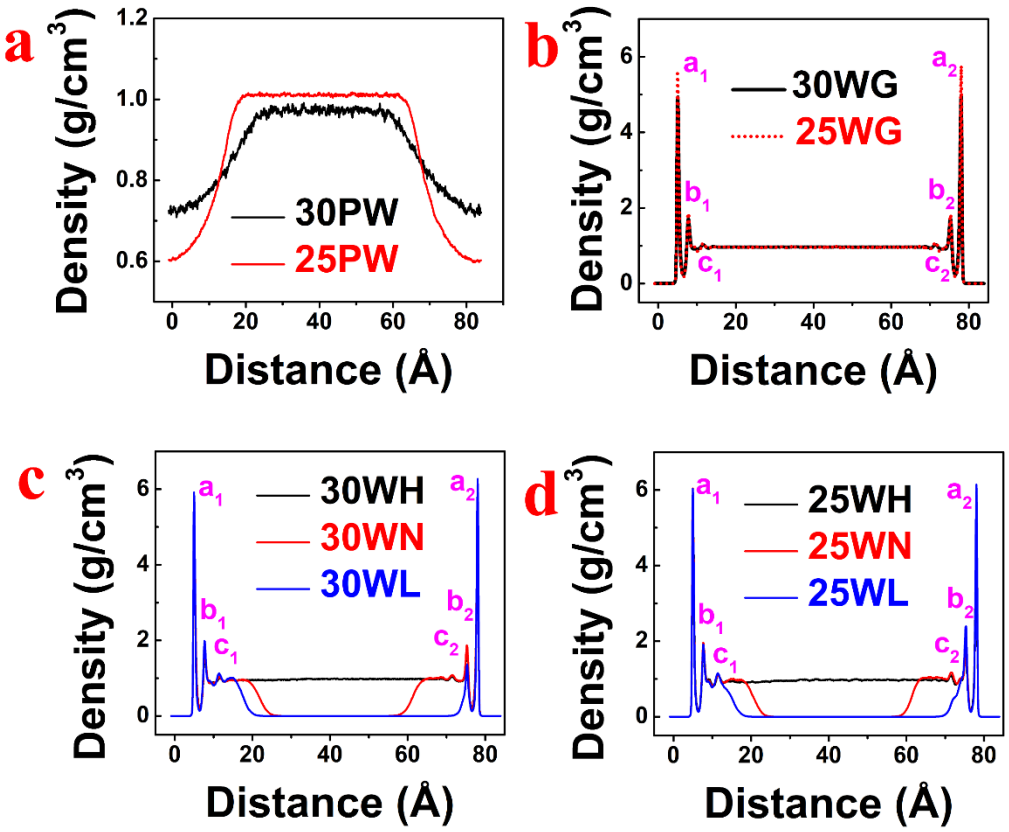


**Figure 2.2.** Density of water by z-axis at temperatures 300 K and 250 K with models – (a) 30PW, 25PW; (b) 30WG, 25WG; (c) 30WH, 30WN, 30WL; (d) 25WH, 25WN, 25WL.

To observe the interaction of water, gold, and polymer, we first investigated the density of water along the z-axis. In Fig. 2.2a, the densities of pure water focus on the horizontal line with oscillating values around 1 g $cm^{-3}$ from 25 to 57 Å and 20 to 63 Å for 30PW and 25PW, respectively. However, in the cases of 30WG and 25WG (Fig. 2.2b), the interaction between the two gold plates and water led to the presence of six peaks: $a_1$, $b_1$, $c_1$, $a_2$, $b_2$, and $c_2$ at the positions of 5.05, 7.75, 11.75, 78.05, 75.35, and 71.35 Å, respectively. Therefore, water is separated into three layers on each gold surface due to the dominance of surface forces, similar to that reported in the literature.[41,42] These forces were extensive on the hydrophilic gold surface, leading to higher peak water density near the gold surface. From 12 to 78 Å, because the interaction occurs between water molecules only, water shows a density around a constant value of 1 g $cm^{-3}$. The zero-density region between the liquid and solid surfaces has been observed both experimentally and mathematically.[43,44] In Fig. 2.2c, the six peaks reappeared in 30WH and

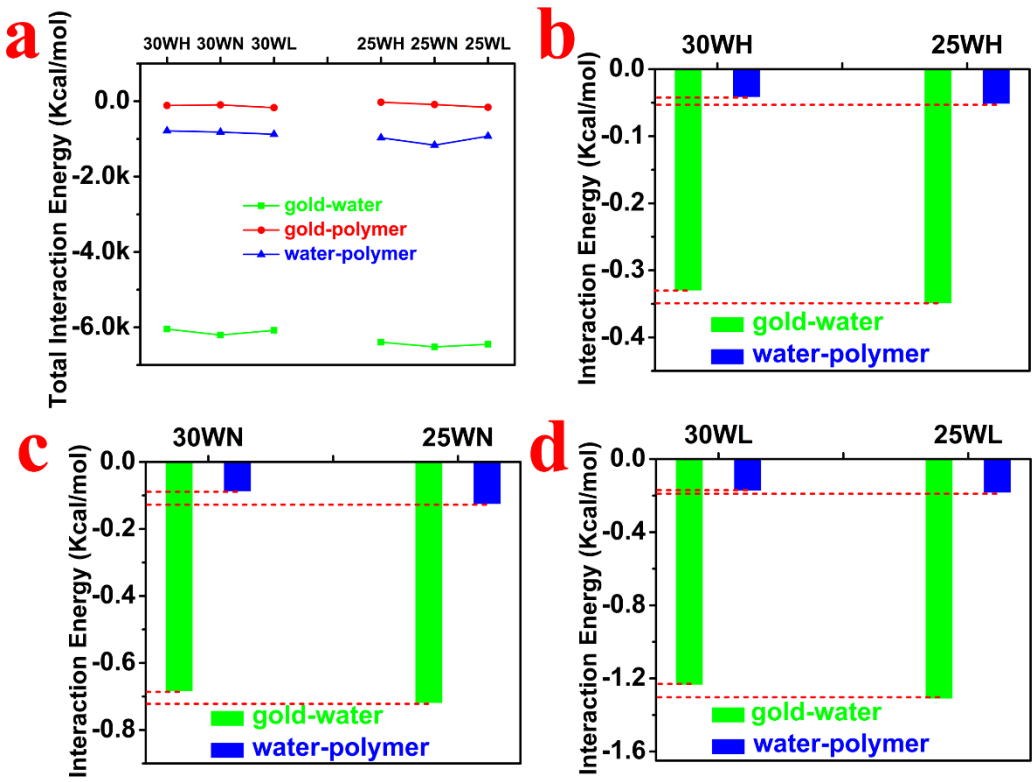


**Figure 2.3.** (a) Total Interaction energy of all atoms gold-water, gold-polymer, and water-polymer at temperatures 300 K for 30WH, 30WN, 30WL and 250 K for 25WH, 25WN, 25WL; (b-d) Comparing interaction energy per water molecule of gold-water and water-polymer (WH, WN, WL) at temperature 300 K and 250 K.

30WN, while 30WL did not have peak $c_2$ due to the low amount of water. There are no water molecules from 24.55 to 68.45 Å in 30WL and 28.55 to 54.75 Å in 30WN. These phenomena similarly occur in 25WH, 25WN, and 25WL (Fig. 2.2d). In Fig. 2.S1 (ESI†), the polymer spreads out from 5 to 34 Å in 25WH and 30WH, and 5 to about 25 Å in the other systems. However, we did not see any clear peak for water density by the interaction between polymer and water in Fig. 2.2c and d. This demonstrates that the interaction between gold and water is stronger than that between polymer and water. For the density of water in the x-axis and y-axis, there are horizontal lines (data not shown).

The above results can be explained by analyzing the total interaction energy between the groups of materials, i.e. gold–water, gold–polymer, and water–polymer (Fig. 2.3a). The interaction energy of gold–water has the

highest value with over – 6000 kcal $mol^{-1}$. However, that of water–polymer is only from –784 to –1164 kcal $mol^{-1}$, and this energy is 5.6 to 7.7 times lower than that of gold–water because the number of polymer atoms is relatively small (723 atoms) compared to gold (3528 atoms). These results explain the disappearance of the peaks of water density for the interaction of polymer and water described in Fig. 2.2. On the other hand, the interaction energy of gold–polymer has the lowest value, which is from –25 to –170 kcal $mol^{-1}$. All the values of energy are shown in Table 2.S1 (ESI†). The temperature variation also affects the interaction energy per water molecule (Fig. 2.3b–d) due to 25WH, 25WN, and 25WL having higher energy than 30WH, 30WN, and 30WL, respectively. Therefore, the variation of temperature impacts the water structure to polymer and gold through different water molecules.

To verify the attractive interaction between polymer and water, we analyzed the distribution of the water molecules around the polymer using the radial distribution function (RDF) between the oxygen atoms of water and the atoms of the polymer. As shown in Fig. 2.4, all six models have the same positions of the four peaks at 1.75, 2.85, 3.75, and 4.85 Å. These peaks indicate that there are four separate regions of water around the polymers. There are no water molecules in the distance of 0 to 1 Å estimated from any atoms of the polymers; therefore, there is no hydrogen bond between water and the polymer. In the distance of 1 to 4 Å, we found three clear peaks. However, in the distance of 4 to 5 Å, the fourth peak is broad, so the fourth region is thinner than the other three regions. For the further distances, there are no peaks and no interaction between polymer and water. Besides, the density of water at each peak of the given system (WH, WN or WL) is also higher at 250 K than at 300 K. These results also match the oxygen atoms of water around the polymer calculated from the last frame (data of the last simulation step) in Fig. 2.S4 (ESI†).

To classify water around the polymer, we analyzed the tetrahedral order of oxygen in water molecules and polymers. Debenedetti and Errington have extensively discussed the orientational order parameter q for 4-coordinated water molecules.[45] A convenient measurement of the local tetrahedral associated with a given oxygen atom i is given by:

$$q_{tet} = 1 - \frac{3}{8}\sum_{j=1}^{3}\sum_{k=j+1}^{4}\left(\cos\theta_{ijk} + \frac{1}{3}\right)^2 \quad (1)$$

where θ is the angle between the bond vectors $r_{ij}$ and $r_{ik}$, and the j and k

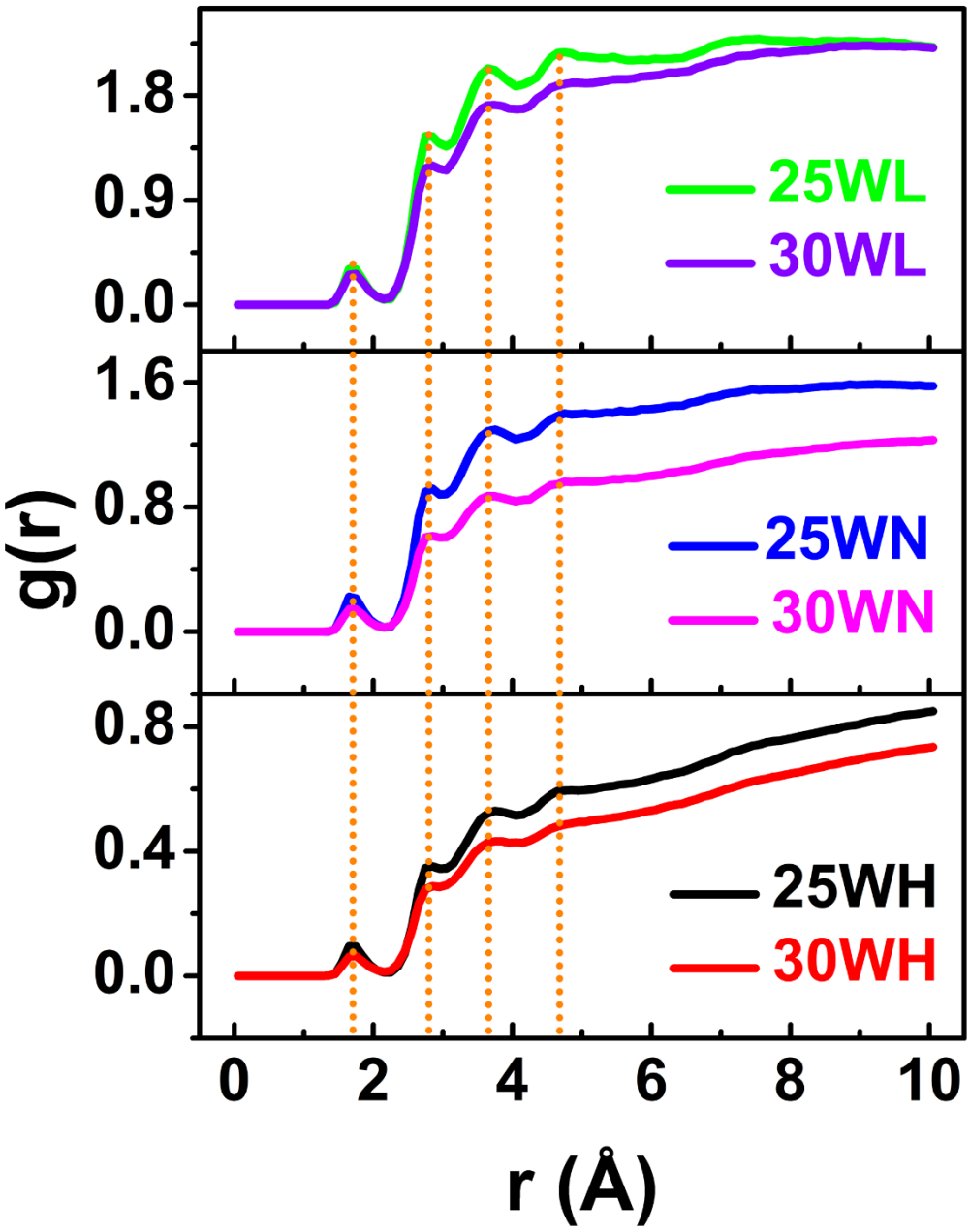


**Figure 2.4.** Radial distribution function (RDF) between the oxygen of water molecules and atoms of polymers

labels are typical for the four nearest oxygen atoms. This formula is the most common type for tetrahedral order parameters.[46–51] This order parameter uses the four closest oxygen neighbors in the water molecules and polymer to calculate. The value of q can range from 0 to 1, where 0 is for the ideal gas or the disorder, and 1 is for perfect tetrahedral structures or the order.

In Fig. 2.5a, we checked the tetrahedral order of the oxygen atoms of water,

and all the models had one prominent peak called $T_1$ at q = 0.5. The sharp peak $T_1$ decreases with increasing amount of water from 30WL to 30WH. This phenomenon is explained by increasing the tetrahedral order of water molecules at $q \geq 0.5$. When a huge amount of water molecules combines with each other to form a tetrahedral geometry, the areas under the curves at $q \geq 0.5$ are more extensive than areas at $q < 0.5$ with the ratios of 1.53, 1.84, 2.2, 2.2, and 2.0 for model 30WL, 30WN, 30WH, 30WG, and 30PW, respectively. The curve of 30WG is similar to that of 30WH due to the same number of water molecules. However, although 30PW has the same number of water molecules as 30WH and 30WG, there is only a broad peak at q = 0.5. This $T_1$ peak shows that under the interaction of gold, the water molecules align to form a tetrahedral order from $q \geq 0.5$. This phenomenon is also observed in Fig. 2.5b. The peak $T_1$ appears in the models 25WL, 25WN, 25WH, and 25WG at q = 0.5, but it nearly disappears in 25PW. Furthermore, another peak $T_2$ appears in all the five models at the lower temperature of 250 K. The position of the peak $T_2$ depends on the number of water molecules in each model. The peaks $T_2$ show up at q = 0.64, 0.71, 0.79, 0.8, and 0.8 for 25WL, 25WN, 25WH, 25WG, and 25PW, respectively. There is a shift of the peak $T_2$ from left to right when the number of water molecules increases from WL to WH. As is well-known, water is transformed from the liquid phase to the ice phase when temperature is below 273 K. In the ice phase, water has structures such as the tetrahedral lattice for the simplest form of ice, Ice I, as mentioned in the literarture.[1,52] Therefore, the proportions of areas with $q \geq 0.5$ and $q < 0.5$ are higher at 250 K than at 300 K with the ratios of 2.3, 2.95, 3.95, 4.0, and 3.8 for models 25WL, 25WN, 25WH, 25WG, and 25PW, respectively. The tetrahedral structure of the ice phase contributes to the explanations for the appearance of the peak $T_2$ at 250 K.

In other studies, scientists revealed that the hydrogen bond interactions by ether and ester groups with water, such as C=O···HOH, C=O···HOH···O=C, and C− O···HOH···O− C, were related to non-freeze water, but C−O···HOH···HOH and C−O···HOH were related to intermediate water.[16,20] In the case of the OH group, Kitano and collaborators surveyed the FT-IR spectra for the O−H stretching band peaks of PEG, including the bonding types such as C−OH···HOH, C−OH···HOH···O−C, and HOH···OH···HOH.[53] From the FT-IR study, if the molecular weight of PEG is low, the OH group can be considered as intermediate water. Similarly, the polymer's molecular

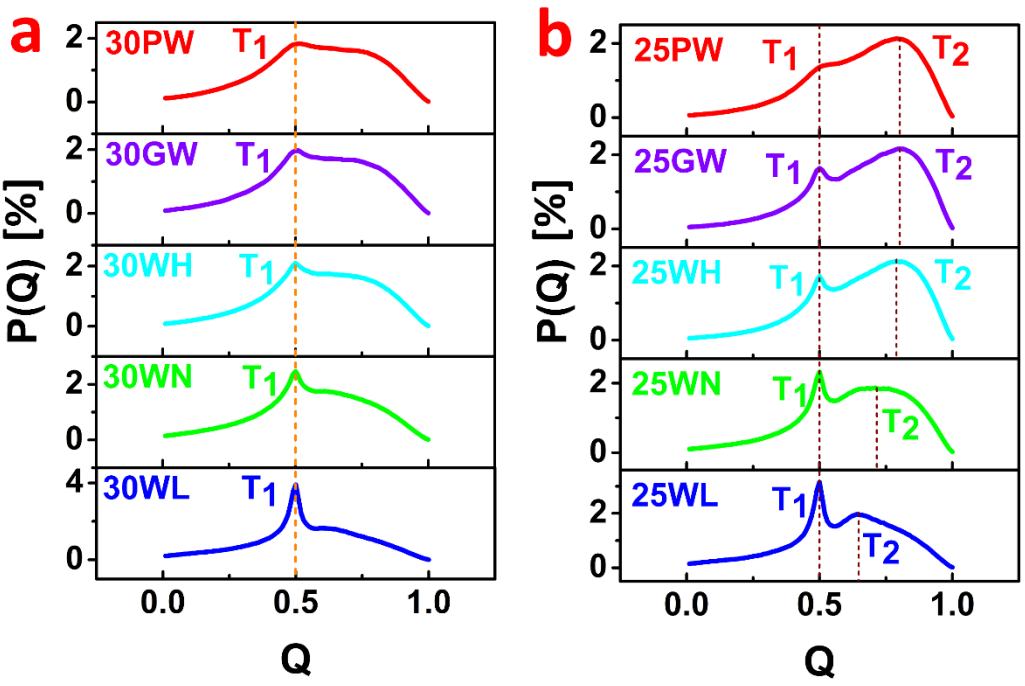


**Figure 2.5.** Orientational Tetrahedral Order of oxygen water. (a) At temperature 300 K for models 30PW, 30WG, 30WH, 30WN, and 30WL; (b) At temperature 250 K for models 25PW, 25WG, 25WH, 25WN, and 25WL

weight is low in our simulation, and the α-CDs also supply many OH groups. In addition, α-CDs are soluble in water, and PEG of low molecular weight is infinitely soluble in water. Therefore, combining all these characteristics and the obtained results, the hydrogen bond between the OH group and water should match with that of intermediate water in our study. Besides, the non-freezing water is not frozen below 273 K, hence it does not have any structures; thus, it is considered the disorder. On the contrary, the intermediate water is freezable below 273 K, hence it has a tetrahedral structure; thus, it is considered the order.

For more detail, we continued to study the tetrahedral order of oxygen, including the oxygen of polymer and oxygen of water around the polymer (Fig. 2.6). The polymer has 133 oxygen atoms, with 53 in the OH group and 80 in the ether and ester groups. Here we surveyed the tetrahedral order not only for the total number of oxygen atoms of the polymer (red curve) with the oxygen atoms of water but also for the oxygen in the OH group (blue curve) or the oxygen in the ether and ester groups (black curve) with the oxygen atoms of water. The red curve represents the sum of the blue curve and the black curve. We also found that the positions of the peaks $T_1$ around

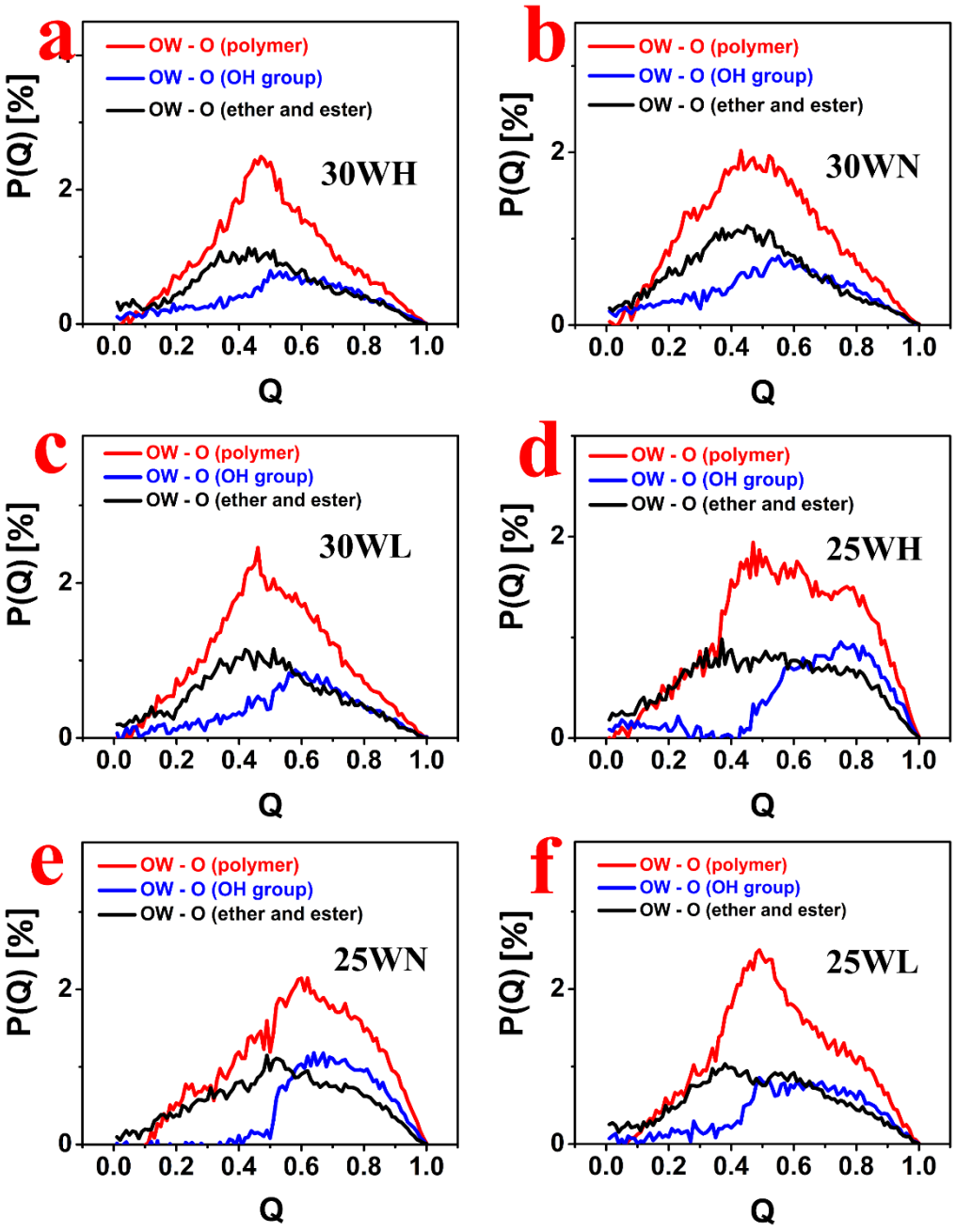


**Figure 2.6.** Orientational Tetrahedral Order at 300 K and 250 K by oxygen in water with total oxygen of polymer (red curve), oxygen in water with oxygen in OH group (blue curve) and oxygen in water with oxygen in ether and ester (black curve). Red curve = blue curve + black curve.

q = 0.5 in 30WH, 30WN, and 30WL had almost symmetric red curves, as seen in Fig. 2.6a–c. This result indicates that the interaction of polymer and water affects the tetrahedral order of oxygen just like the interaction of gold and water. As shown in Fig. 2.6d–f, the red curves tend to order when the

temperature is 250 K, as observed for the tetrahedral order of water in Fig. 2.5.

Meanwhile, at 300 K, the blue curves tend to order and the black curves tend to disorder (Fig. 2.6a–c). However, at 250 K, the blue curves tend to order totally and the black curves tend to be a half disorder and a half order (Fig. 2.6d–f). Therefore, the blue and black curves conform with other studies.[16,20,53] The interaction of oxygen in the OH group with water corresponds to intermediate water, whereas that in the ether and ester groups with water corresponds to intermediate water and non-freezing water in our study, respectively.

With the results in Fig. 2.5 and 2.6, we continue to categorize the water molecules based on the position of peak $T_1$ at $q = 0.5$, to study the width and distance of each type of water around the polymer. Water molecules belonging to $q \geq 0.5$, were classified as the order, while others are the disorder with $q < 0.5$. Hence, water is classified based on the distance from its oxygen atoms to the polymer atoms (Fig. 2.7). Here, the last frame in the equilibrium simulation of eight relaxation nanoseconds was considered for the calculations. We focused on water molecules around the polymer at 5 Å due to the four water regions formed around it at this distance, as described in Fig. 2.4. Again, there are no water molecules in the distance from 0 to 1 Å. With the distance from 1 to 2 Å, the percentage of water molecules belonging to the disorder is more dominant than those with the order for all models. This result means that the first region should be non-freezing water.

In the distance from 2 to 3 Å, the disorder of the water molecules (68%) in 30WH, 30WN, or 30WL is more than double their order (32%). However, with the models 25WH and 25WN, the percentage of the disorder and order are pretty equal. When the temperature decreases from 300 K to 250 K, the water molecules tend to change from disorder to an equilibrium situation between disorder and order. Therefore, the second region is an interference area of non-freezing and intermediate water in the distance from 2 to 3 Å. In 25WL, due to the lack of water molecules covering all the polymers, especially the CDs, the order of the water molecules (37%) is lower than the disorder (63%).

In the distance from 3 to 5 Å, the order percentage is higher than the disorder percentage for all models. However, the total water molecules, including their order and disorder, from 3 to 4 Å are higher than the total water molecules from 4 to 5 Å (Fig. 2.S4, ESI†). Hence, the third region

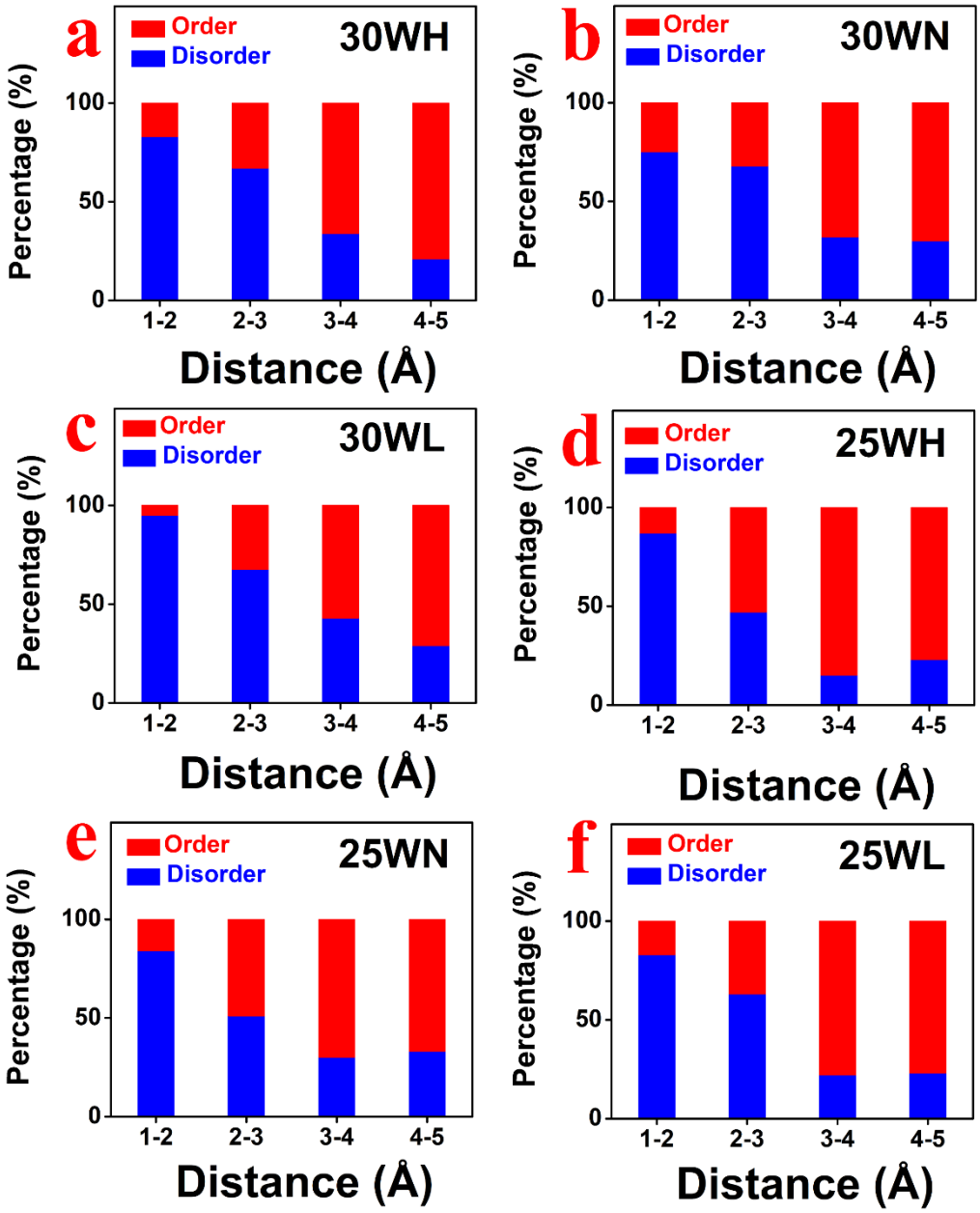


**Figure 2.7.** The percentage (%) of oxygen waters which reside in Order and Disorder by shortest distance to polyrotaxane at temperature 300 K for models (a) 30WH; (b) 30WN; (c) 30WL; and 250 K for models (d) 25WH; (e) 25WN; (f) 25WL

should belong to intermediate water in the distance from 3 to 4 Å. The fourth region is an interference area of intermediate water and free water because it is a thin region (Fig. 2.4), and has the lowest number of oxygen atoms of water (Fig. 2.S4, ESI†). A distance greater than 5 Å means that water molecules are related to free water.

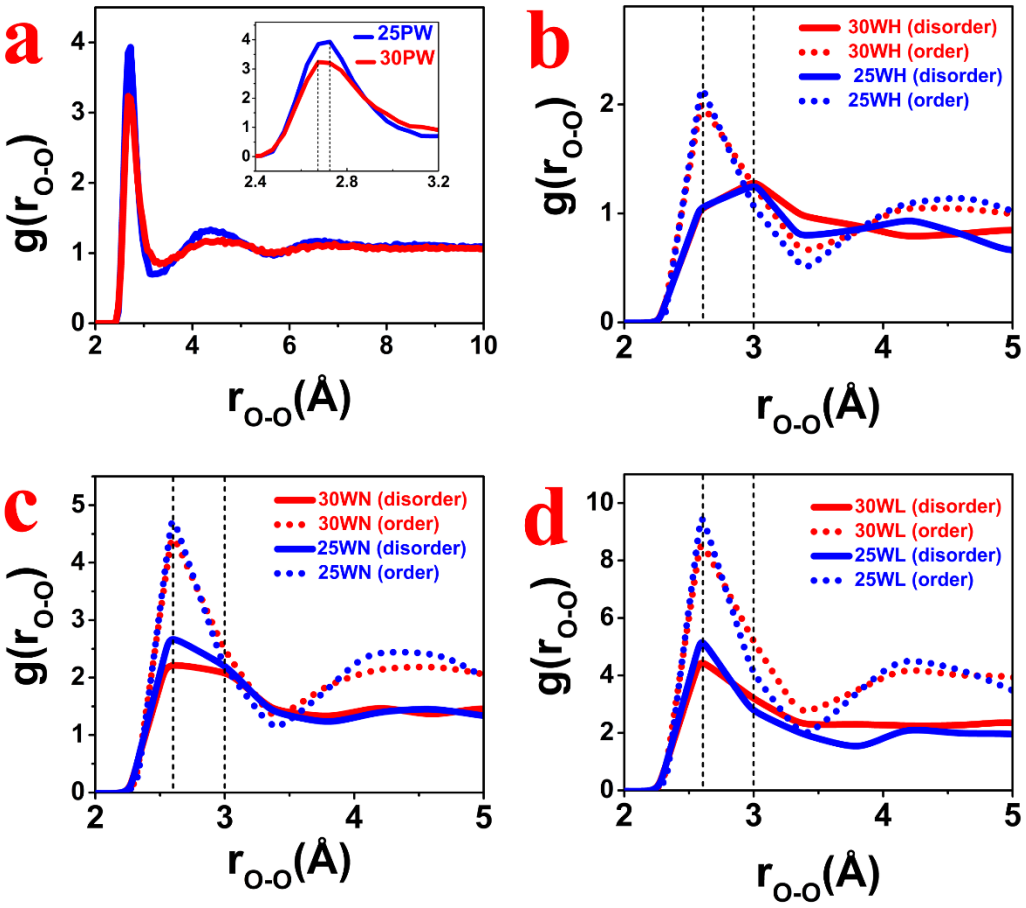


**Figure 2.8.** Radial Distribution Function (RDF) of oxygen water. a) 30PW and 25PW; (b-d) oxygen water of disorder and order in models with (b) 30WH and 25WH; (c) 30WN and 25WN; (d) 30WL and 25WL.

To further investigate water's structural properties, we calculated the RDF of water molecules ($g_{OO}$) that are typical for order and disorder, based on Fig. 2.7. Firstly, the last frame of pure water was examined at 300 K and 250 K (Fig. 2.8a). The first peak of 25PW is slightly higher than that of 30PW on the x-axis. This result shows that the density of water at 250 K is lower than that at 300 K. This observation is consistent with reality. However, there is no difference between 30PW and 25PW (Fig. 2.S3, ESI†) for the first peak when RDF is averaged over the last 100 frames, and the averaged RDF lines are also smoother than those of one frame (Fig. 2.8a). By checking the last frame in Fig. 2.8b–d, all the sharp peaks of order water molecules are at 2.6 Å in all the models. Disorder water molecules have broad peaks from 2.6 to 3 Å (Fig. 2.8b and c). However, when the amount of water decreases from WH to WN, the highest peaks of disorder water

molecules shift from 3 to 2.6 Å. In the case of the low water amount, the peaks of disorder water molecules completely change from broad peaks to a sharp peak at 2.6 Å (Fig. 2.8d). As a result, the density of disorder water molecules is lower than that of the order ones. In addition, the height of the order and disorder peaks at 250 K is higher than at 300 K (Fig. 2.8c and d). However, as shown in Fig. 2.8b, the disorder peaks at 250 K and 300 K are the same. There is a slight difference in the height of the order peak at 300 K and 250 K. These results imply that the classification of types of water depends on the temperature and amount of water around the polymer.

Besides, the hydrogen bond between polymer and water and the hydrogen bond between water and water were investigated by analyzing the trajectory of this interaction; in geometric criteria, an acceptor–donor distance is lower than 3.5 Å, and an angle of donor–hydrogen–acceptor is less than 351 (Fig. 2.S2, ESI†). The number of hydrogen bonds at 250 K is higher than that at 300 K for all the six models (Fig. 2.S2a–c, ESI†). These results are similar to the increasing tetrahedral order seen in Fig. 2.6 and 2.7 when the temperature is below 273 K. Therefore, water molecules should arrange into a tetrahedral-like lattice structure or increase the order in the ice phase. As shown in Fig. 2.S2d (ESI†), the ratios of the total average number of water–water hydrogen bonds among WH, WN, and WL are 1 : 0.487 : 0.263 at 300 K and 1 : 0.484 : 0.258 at 250 K. These ratios are proportional to the ratio of water molecules among WH, WN, and WL, i.e. 1 : 0.495 : 0.268. The number of hydrogen bonds between water and the polymer depends on the torsion and curvature of the polymer, and thus it fluctuates. As a result, the maximum values cannot be obtained to compare with those of the total 133 oxygen atoms of the polymer (Fig. 2.S2a–d, ESI†).

**Relationship between tetrahedral order and XES spectra**

T. Tokushima and colleagues showed two peaks ($1b_1$' and $1b_1$'') of the O 1s XES spectra of liquid water over the temperature range of 280 to 338 K.[40] With crystalline ice, E. Gilberg and colleagues revealed a dominant peak $1b_1$' and unclear peak $1b_1$''.[39] These two peaks are related to four-fold ($1b_1$') and less than four-fold ($1b_1$'') H-bonded structures in the water. For water in the electrolyte brush, K. Yamazoe and colleagues exhibited only one peak $1b_1$' in their study.[13] However, with heavy water ($D_2O$) in 3-methylpyridine, H. Arai and colleagues reported that, depending on the ratios of $D_2O$ in solution from high to low, the intensity of peak $1b_1$' decreased while that of peak $1b_1$'' increased.[14] In another study of D2O in

organic solvents, T. Tokushima and colleagues showed similar results.[15]

In our study, the water model TIP3P/B might be obtained with a more tetrahedral HOH angle by calculating long-range electrostatic interactions. The tetrahedral order is one of the four-fold structures that increases when the temperature is below 273 K. Therefore, we considered $1b_1$' as the order and $1b_1$'' as the disorder in our study on tetrahedral order. Besides, the tetrahedral order shows two peaks in the XES spectra (Fig. 5b). We see the similarity between the peaks $T_2$ and $T_1$ of 25PW and $1b_1$' and $1b_1$'' of crystalline ice, respectively. With 30PW (Fig. 2.5a), $T_1$ appears more clearly than $T_2$. This phenomenon shows that the water molecule tetrahedral geometries significantly increase, but these structures are not as close to perfect tetrahedral structures as those of 25PW. Therefore, $T_2$ is not distinct in 30PW, although there is a sizeable tetrahedral order with $q \geq 0.5$. For the ratios of water in systems from low (WL) to high (WH/WG), the intensity of peak $T_1$ decreased at 250 K and 300 K while that of peak $T_2$ increased, especially at 250 K for all systems. These results were similar to the abovementioned experimental studies.

With the interaction between chemical groups of polymers and water shown in Fig. 2.6, the tetrahedral order can be utilized to predict the XES spectra. The two peaks $1b_1$' and $1b_1$'' can be recognized depending on the ratio of the number of OH groups (order) to ether and ester groups (disorder) in the polymer, the amount of water, and the temperature. It should be possible to view two peaks $1b_1$' and $1b_1$'' at 250 K in Fig. 2.6d–f, or only a broad peak from the emission energy position of $1b_1$' to $1b_1$'' at 300 K in Fig. 2.6a–c due to the asymmetry or symmetry of the red curves. Therefore, we hope for more data from the XES experiments to classify the types of water in the future. Furthermore, the combination of tetrahedral order in simulation and XES can categorize the water types in more detail to compare with other known methods.

**Simulation section**

Each simulation box with a size of $x \times y \times z = 85 \times 85 \times 85$ Å$^3$ contains one PR and the water molecules inserted between the two Au plates (Fig. 2.1). Each Au plate of 1764 atoms has the sizes in the x- and y-directions equal to those of the box and the two atomic layers in the z-direction. One PR, which is described in detail in Fig. 2.1, includes three α-CDs, three ALA linkers and one PEG chain of 38 monomers. In the initial configurations, the three systems WH, WN, and WL contain 18225, 9025 and 4900 water

molecules, respectively, which are regularly arranged along the directions with constant distances of (x, y, z) = (3.1, 3.1, 3.1), (4.3, 4.3, 3.1) and (6.1, 6.1, 3.1) Å, respectively. The ratio of water molecules among WH, WN, and WL is 1 : 0.495 : 0.268. General AMBER Force Field (GAFF) parameters are used to describe the interactions between the atoms of the PR. The atomic partial charges for the α-CDs and ALA linkers were taken from density functional theory calculations using the B3LYP/6-31G(d,p) by Gaussian software.[54] Those of PEG were calculated from AM1-BCC by Antechamber.[55,56] GolPCHARMM parameters for the interactions of Au–Au, Au–water and Au–S (thio) were taken from the literature.[57] Lorentz–Berthelot rules are used to calculate the interaction parameters between two unrelated non-bonded atoms. Long-range Coulombic interactions are computed in particle–particle–particle-mesh (pppm) K-space. All atomistic simulations were performed with the LAMMPS package.[58] Each system is under NVT canonical ensemble behavior and periodic boundary conditions in the x- and y-directions. The atoms of the Au plates are fixed during the simulations. Temperature is controlled by the Nose–Hoover thermostat method. Properties of each system are detected at the two different temperatures of 250 and 300 K for comparison. The equations of motion are integrated using the velocity-Verlet algorithm with a time step of 1 fs. Each simulation is run in the time of 8 ns and the obtained values are averaged over this time. After 8 ns, the simulations achieve equilibrium by temperature, total energy, and the radius of gyration of the polymer (data not shown).

**2.4 Conclusions**

In summary, we have demonstrated that our simulation study successfully classifies non-freezing water and intermediate water based on the analysis of the tetrahedral order of water molecules around a polymer in the distance from 1 to 5 Å, by observing four separate regions. The first region is the nearest distance to the polymer and belongs to non-freezing water. The second region is an interference area of non-freezing water and intermediate water. The third region belongs to intermediate water. The fourth region is an interference area of intermediate and free water due to the polymer and water's weak interaction and is the thinnest region. Beyond a distance of 5 Å, water molecules are considered free water.

## 2.5 Support Information

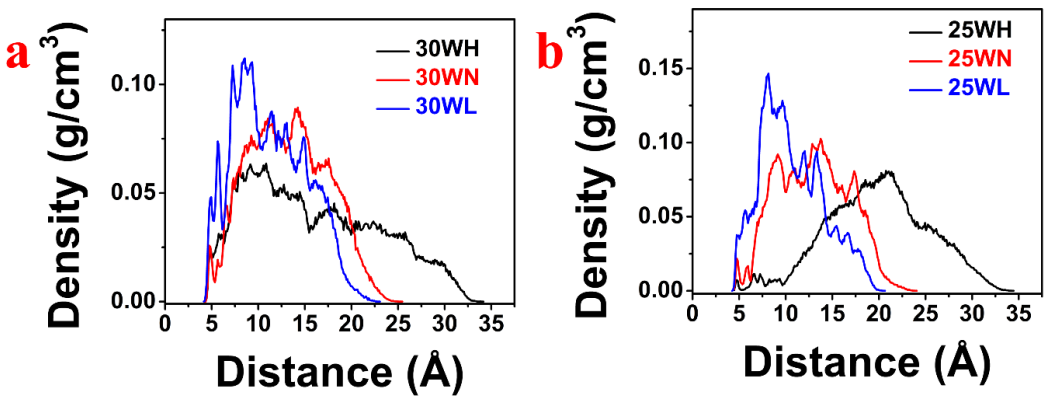


**Figure 2.S1.** Density of polymer by z-axis at temperatures 300 K and 250 K with models – (a) 30WH, 30WN, 30WL; (b) 25WH, 25WN, 25WL.

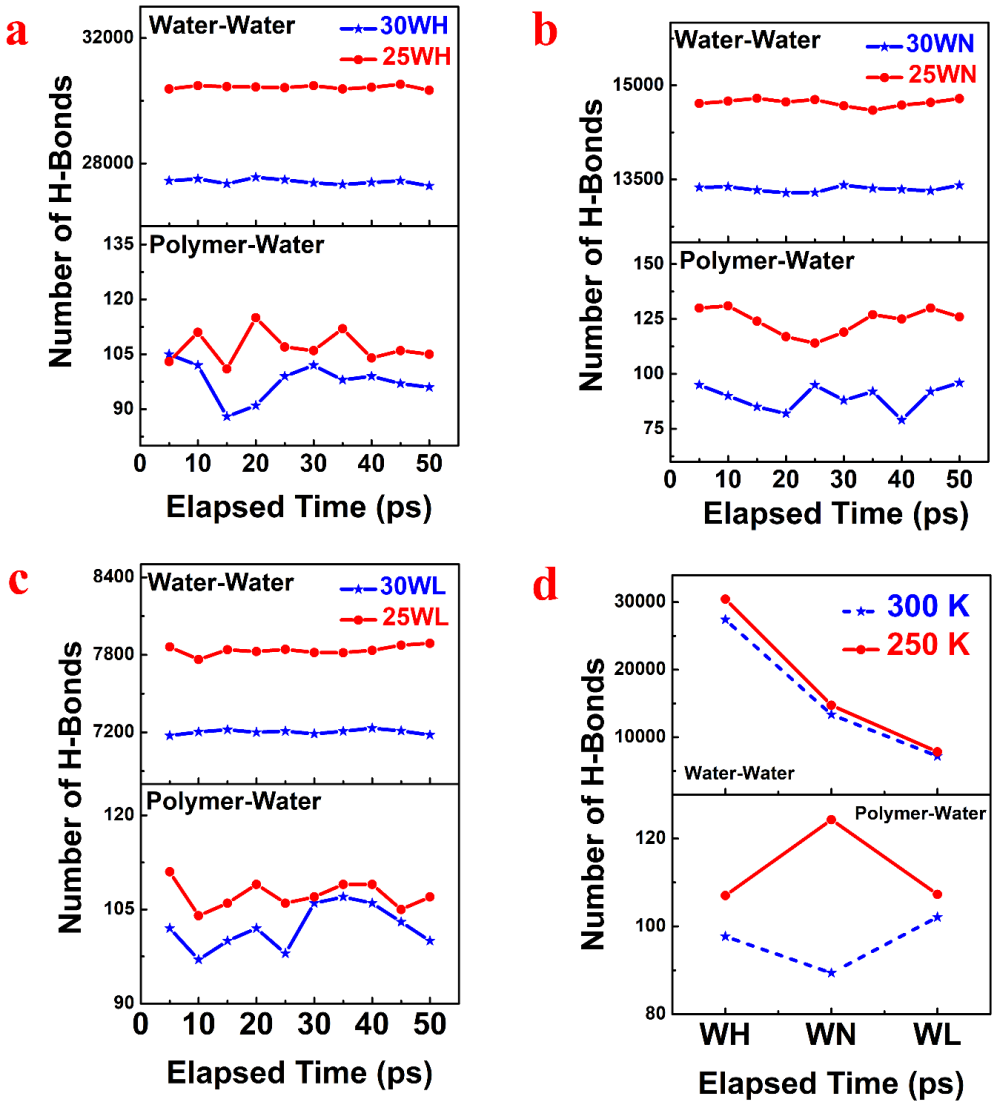


**Figure 2.S2.** Number of H-Bonds at 300 K and 250 K. (a) 30WH and 25WH; (b) 30WN and 25WN; (c) 30WL and 25WL; (d) total average H-bonds of WH, WN, and WL. Water-Water is number H-Bonds between water and water. Polymer-Water is number of H-Bonds between polymer and water.

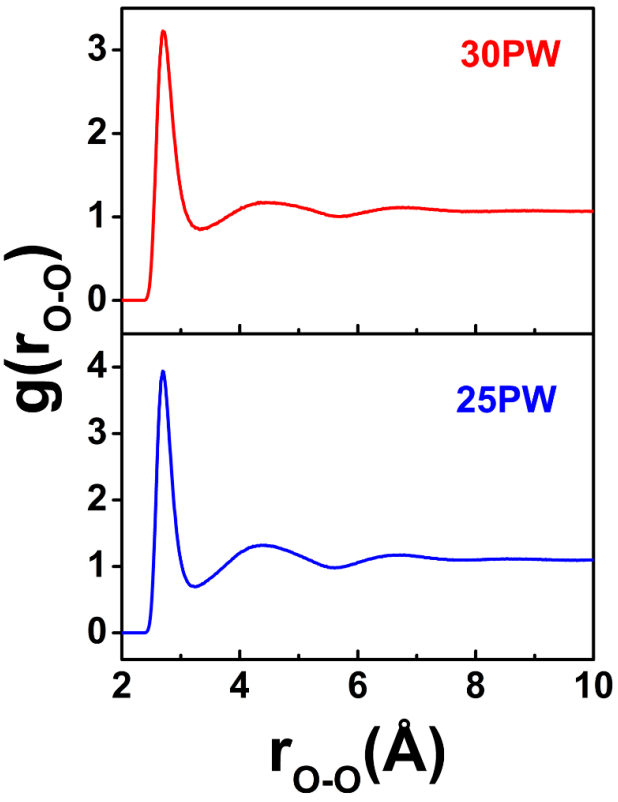


**Figure 2.S3.** Radial Distribution Function (RDF) of oxygen water in models 30PW and 25PW with 100 frames

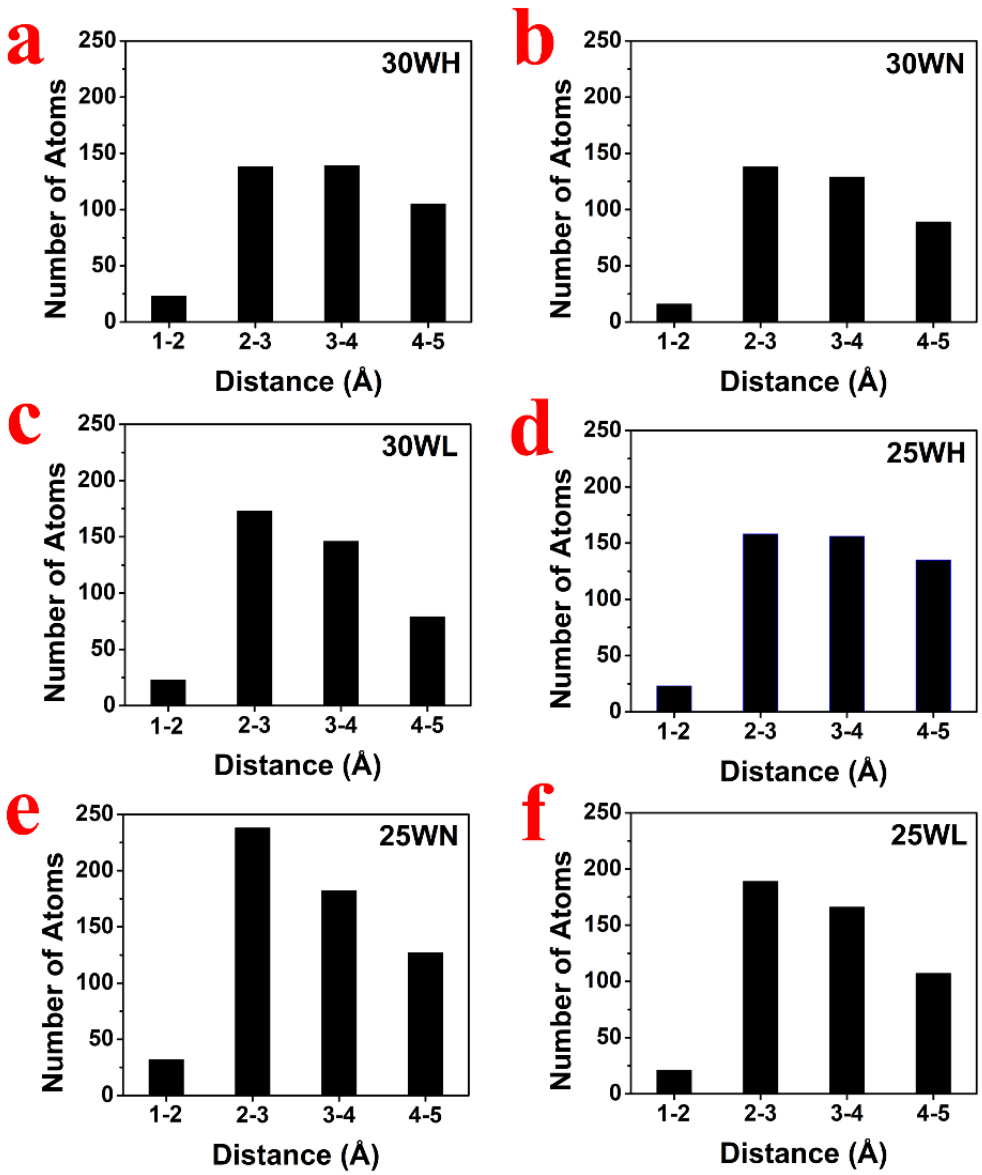


**Figure 2.S4.** Number of oxygen atoms around polyrotaxane in the last frame at 300 K and 250 K for WH, WN, and WL systems.

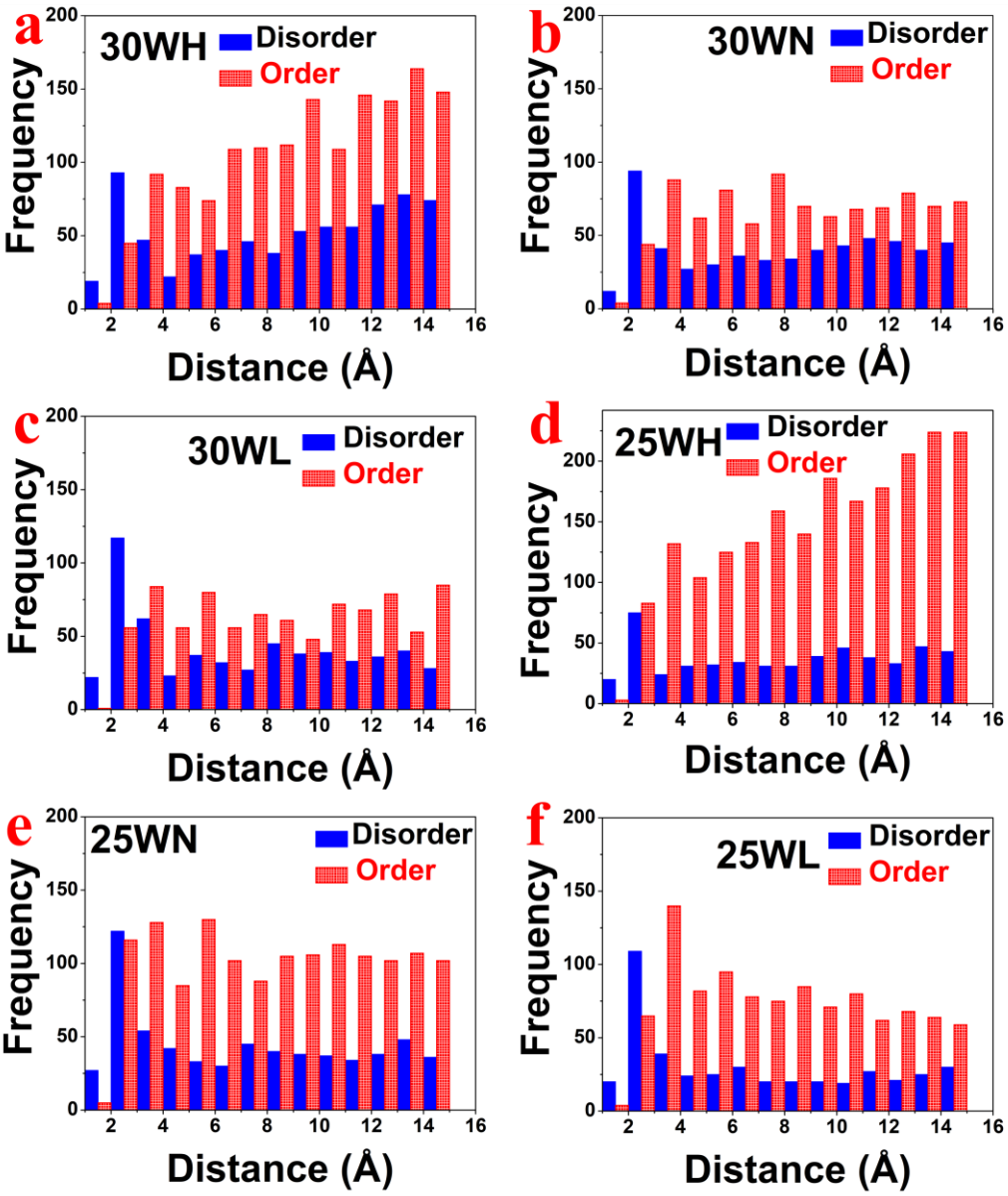


**Figure. 2.S5.** The number of oxygen waters which reside in Order and Disorder by shortest distance to polyrotaxane at temperature 300 K for models (a) 30WH; (b) 30WN; (c) 30WL; and 250 K for models (d) 25WH; (e) 25WN; (f) 25WL.

**Table 2.S1.** Total interaction energy (Kcal $mol^{-1}$) of all atoms: gold-water, gold-polymer, and water-polymer at temperatures 300 K for 30WH, 30WN, 30WL, and 250 K for 25WH, 25WN, 25WL

| Models | Gold-Water | Gold-Polymer | Water-Polymer |
|---|---|---|---|
| **30WH** | -6,045.17 | -112.278 | -783.734 |
| **30WN** | -6,204.9 | -95.9814 | -819.3 |
| **30WL** | -6,079.66 | -169.729 | -876.484 |
| **25WH** | -6,395.27 | -24.527 | -968.668 |
| **25WN** | -6,518.28 | -86.4425 | -1,163.7 |
| **25WL** | -6,449.24 | -159.483 | -925.771 |

**Table 2.S2.** System specifics of all models

| Name Sample | Number of Polymer | Water Molecules | Each plate of gold | Temperature |
|---|---|---|---|---|
| **30WH** | 1 chain PEG, 3 CDs, 3 Linkers | 18,225 molecules | 1,764 atoms | 300 K |
| **30WN** | 1 chain PEG, 3 CDs, 3 Linkers | 9,025 molecules | 1,764 atoms | 300 K |
| **30WL** | 1 chain PEG, 3 CDs, 3 Linkers | 4,900 molecules | 1,764 atoms | 300 K |
| **30WG** | none | 18,225 molecules | 1,764 atoms | 300 K |
| **30PW** | none | 18,225 molecules | none | 300 K |
| | | | | |
| **25WH** | 1 chain PEG, 3 CDs, 3 Linkers | 18,225 molecules | 1,764 atoms | 250 K |
| **25WN** | 1 chain PEG, 3 CDs, 3 Linkers | 9,025 molecules | 1,764 atoms | 250 K |
| **25WL** | 1 chain PEG, 3 CDs, 3 Linkers | 4,900 molecules | 1,764 atoms | 250 K |
| **25WG** | none | 18,225 molecules | 1,764 atoms | 250 K |
| **25PW** | none | 18,225 molecules | none | 250 K |

**Table 2.S3.** Averaged charges of atoms. The α-CD and ALA linker were taken from density functional theory calculations using the B3LYP/6-31G(d,p) by Gaussian software. For PEG, the atomic partial charges were calculated from AM1-BCC by Antechamber.

**CD+linker**

| Type atom | Charge |
|---|---|
| c3 | 0.165558 |
| h1 | 0.045993 |
| h2 | 0.099463 |
| hc | 0.041664 |
| ho | 0.409587 |
| oh | -0.6091 |
| os | -0.49723 |
| ss | -0.13224 |
| c | 0.721409 |
| o | -0.52741 |

**PEG**

| Type atom | Charge |
|---|---|
| c3 | 0.126092 |
| h1 | 0.043854 |
| ho | 0.4015 |
| oh | -0.6028 |
| os | -0.42826 |

**References**

1. W. S. Benedict, N. Gailar and E. K. Plyler, Rotation-Vibration Spectra of Deuterated Water Vapor, J. Chem. Phys., 1956, 24, 1139–1165.

2. R. Podgornik, Water and life: the unique properties of H(2)O: Ruth M. Lynden-Bell, Simon Conway Morris, John D. Barrow, John L. Finney and Charles Harper (eds). CRC Press; 1 edition, 2010, J. Biol. Phys., 2011, 37, 163–165.

3. B. Bagchi, Water in Biological and Chemical Processes: From Structure and Dynamics to Function, Cambridge University Press, Cambridge, 2013.

4. P. Ball, Life's Matrix: A Biography of Water, University of California Press, 2001.

5. A. A. Darhuber and S. M. Troian, Principles of microfluidic actuation by modulation of surface stresses, Annu. Rev. Fluid Mech., 2005, 37, 425–455.

6. V. Srinivasan, V. K. Pamula and R. B. Fair, An integrated digital microfluidic lab-on-a-chip for clinical diagnostics on human physiological fluids, Lab Chip, 2004, 4, 310–315.

7. S. Kobayashi, M. Wakui, Y. Iwata and M. Tanaka, Poly(omethoxyalkyl acrylate)s: Nonthrombogenic Polymer Family with Tunable Protein Adsorption, Biomacromolecules, 2017, 18, 4214–4223.

8. K. Sato, S. Kobayashi, M. Kusakari, S. Watahiki, M. Oikawa, T. Hoshiba and M. Tanaka, The Relationship Between Water Structure and Blood Compatibility in Poly(2-methoxyethyl Acrylate) (PMEA) Analogues, Macromol. Biosci., 2015, 15, 1296–1303.

9. A. Nilsson, D. Nordlund, I. Waluyo, N. Huang, H. Ogasawara, S. Kaya, U. Bergmann, L. Å. Na ¨slund, H. O¨stro¨m, P. Wernet, K. J. Andersson, T. Schiros and L. G. M. Pettersson, X-ray absorption spectroscopy and X-ray Raman scattering of water and ice; an experimental view, J. Electron Spectrosc. Relat. Phenom., 2010, 177, 99–129.

10. P. Ball, Water as an Active Constituent in Cell Biology, Chem. Rev., 2008, 108, 74–108.

11. H. Washizu, S. Sanda, S.-a. Hyodo, T. Ohmori, N. Nishino and A. Suzuki, Molecular dynamics simulations of elastohydrodynamic lubrication and boundary lubrication for automotive tribology, J. Phys.: Conf. Ser., 2007, 89, 012009.

12. Y. Ishii, N. Matubayasi, G. Watanabe, T. Kato and H. Washizu, Molecular insights on confined water in the nanochannels of self-assembled ionic liquid crystal, Sci. Adv., 2021, 7, eabf0669.

13. K. Yamazoe, Y. Higaki, Y. Inutsuka, J. Miyawaki, Y.-T. Cui, A. Takahara and Y. Harada, Enhancement of the HydrogenBonding Network of Water Confined in a Polyelectrolyte Brush, Langmuir, 2017, 33, 3954–3959.
14. H. Arai, Y. Horikawa, K. Sadakane, T. Tokushima, Y. Harada, Y. Senba, H. Ohashi, Y. Takata and S. Shin, Hydrogen bonding of water in 3-methylpyridine studied by O 1s X-ray emission and absorption spectroscopy, Phys. Chem. Chem. Phys., 2012, 14, 1576–1580.
15. T. Tokushima, Y. Horikawa, O. Takahashi, H. Arai, K. Sadakane, Y. Harada, Y. Takata and S. Shin, Solvation dependence of valence electronic states of water diluted in organic solvents probed by soft X-ray spectroscopy, Phys. Chem. Chem. Phys., 2014, 16, 10753–10761.
16. T. Tsuruta, On the Role of Water Molecules in the Interface between Biological Systems and Polymers, J. Biomater. Sci., Polym. Ed., 2010, 21, 1831–1848.
17. M. Tanaka and A. Mochizuki, Effect of water structure on blood compatibility—thermal analysis of water in poly- (meth)acrylate, J. Biomed. Mater. Res., Part A, 2004, 68A, 684–695.
18. A.-T. Kuo, S. Urata, R. Koguchi, K. Yamamoto and M. Tanaka, Analyses of equilibrium water content and blood compatibility for Poly(2-methoxyethyl acrylate) by molecular dynamics simulation, Polymer, 2019, 170, 76–84.
19. M. A. Bag and L. M. Valenzuela, Impact of the Hydration States of Polymers on Their Hemocompatibility for Medical Applications: A Review, Int. J. Mol. Sci., 2017, 18, 1422.
20. M. Tanaka, T. Hayashi and S. Morita, The roles of water molecules at the biointerface of medical polymers, Polym. J., 2013, 45, 701–710.
21. K. Nakamura, T. Hatakeyama and H. Hatakeyama, Relationship between hydrogen bonding and bound water in polyhydroxystyrene derivatives, Polymer, 1983, 24, 871–876.
22. Z. E. Hughes, G. Wei, K. L. M. Drew, L. Colombi Ciacchi and T. R. Walsh, Adsorption of DNA Fragments at Aqueous Graphite and Au(111) via Integration of Experiment and Simulation, Langmuir, 2017, 33, 10193–10204.
23. N. Isa, K. D. Gibson, T. Yan, W. Hase and S. J. Sibener, Experimental and simulation study of neon collision dynamics with a 1-decanethiol monolayer, J. Chem. Phys., 2004, 120, 2417–2433.
24. C.-D. Wu, L.-M. Kuo, S.-J. Lin, T.-H. Fang and S.-F. Hsieh, Effects of temperature, size of water droplets, and surface roughness on nanowetting properties investigated using molecular dynamics simulation, Comput. Mater.

Sci., 2012, 53, 25–30.
25. Q. Yuan and Y.-P. Zhao, Precursor Film in Dynamic Wetting, Electrowetting, and Electro-Elasto-Capillarity, Phys. Rev. Lett., 2010, 104, 246101.
26. G. Wenz, B.-H. Han and A. Mu¨ller, Cyclodextrin Rotaxanes and Polyrotaxanes, Chem. Rev., 2006, 106, 782–817.
27. Y. Arisaka and N. Yui, Polyrotaxane-based biointerfaces with dynamic biomaterial functions, J. Mater. Chem. B, 2019, 7, 2123–2129.
28. Y. Sakai, R. Gomi, K. Kato, H. Yokoyama and K. Ito, Structure and dynamics of polyrotaxane-based sliding graft copolymers with alkyl side chains, Soft Matter, 2013, 9, 1895–1901.
29. Y. Koyama, Synthesis of topologically crosslinked polymers with rotaxane-crosslinking points, Polym. J., 2014, 46, 315–322.
30. L. Xie, K.-Y. Chan and N. Quirke, Poly(ethylene glycol) (PEG) in a Polyethylene (PE) Framework: A Simple Model for Simulation Studies of a Soluble Polymer in an Open Framework, Langmuir, 2017, 33, 11746–11753.
31. K. Uchida, Y. Hoshino, A. Tamura, K. Yoshimoto, S. Kojima, K. Yamashita, I. Yamanaka, H. Otsuka, K. Kataoka and Y. Nagasaki, Creation of a mixed poly(ethylene glycol) tethered-chain surface for preventing the nonspecific adsorption of proteins and peptides, Biointerphases, 2007, 2, 126–130.
32. K. Yoshimoto, T. Hirase, J. Madsen, S. P. Armes and Y. Nagasaki, Non-Fouling Character of Poly[2-(methacryloyloxy)ethyl Phosphorylcholine]-Modified Gold Surfaces Fabricated by the ‘Grafting to’ Method: Comparison of its Protein Resistance with Poly(ethylene glycol)-Modified Gold Surfaces, Macromol. Rapid Commun., 2009, 30, 2136–2140.
33. J. M. Harris and R. B. Chess, Effect of pegylation on pharmaceuticals, Nat. Rev. Drug Discovery, 2003, 2, 214–221.
34. T. Hu, B. N. Manjula, D. Li, M. Brenowitz and S. A. Acharya, Influence of intramolecular cross-links on the molecular, structural and functional properties of PEGylated haemoglobin, Biochem. J., 2007, 402, 143–151.
35. V. Berejnov, N. S. Husseini, O. A. Alsaied and R. E. Thorne, Effects of cryoprotectant concentration and cooling rate on vitrification of aqueous solutions, J. Appl. Crystallogr., 2006, 39, 244–251.
36. M.-B. Lascombe, M.-L. Milat, J.-P. Blein, F. Panabieres, M. Ponchet and T. Prange, Crystallization and preliminary X-ray studies of oligandrin, a sterol-carrier elicitor from Pythium oligandrum, Acta Crystallogr., Sect. D: Biol. Crystallogr., 2000, 56, 1498–1500.
37. S. A. Acharya, V. N. Acharya, N. D. Kanika, A. G. Tsai, M. Intaglietta and

B. N. Manjula, Non-hypertensive tetraPEGylated canine haemoglobin: correlation between PEGylation, O2 affinity and tissue oxygenation, Biochem. J., 2007, 405, 503–511.
38. D. J. Price and C. L. Brooks III, A modified TIP3P water potential for simulation with Ewald summation, J. Chem. Phys., 2004, 121, 10096–10103.
39. E. Gilberg, M. J. Hanus and B. Foltz, Investigation of the electronic structure of ice by high resolution x-ray spectroscopy, J. Chem. Phys., 1982, 76, 5093–5097.
40. T. Tokushima, Y. Harada, O. Takahashi, Y. Senba, H. Ohashi, L. G. M. Pettersson, A. Nilsson and S. Shin, High resolution X-ray emission spectroscopy of liquid water: The observation of two structural motifs, Chem. Phys. Lett., 2008, 460, 387–400.
41. A. Pham, M. Barisik and B. Kim, Pressure dependence of Kapitza resistance at gold/water and silicon/water interfaces, J. Chem. Phys., 2013, 139, 244702.
42. C. T. Nguyen, M. Barisik and B. Kim, Wetting of chemically heterogeneous striped surfaces: Molecular dynamics simulations, AIP Adv., 2018, 8, 065003.
43. M. Maccarini, R. Steitz, M. Himmelhaus, J. Fick, S. Tatur, M. Wolff, M. Grunze, J. Janec ˇek and R. R. Netz, Density Depletion at Solid——————————Liquid Interfaces: a Neutron Reflectivity Study, Langmuir, 2007, 23, 598–608.
44. S. I. Mamatkulov, P. K. Khabibullaev and R. R. Netz, Water at Hydrophobic Substrates: Curvature, Pressure, and Temperature Effects, Langmuir, 2004, 20, 4756–4763.
45. J. R. Errington and P. G. Debenedetti, Relationship between structural order and the anomalies of liquid water, Nature, 2001, 409, 318–321.
46. J. Lu, Y. Qiu, R. Baron and V. Molinero, Coarse-Graining of TIP4P/2005, TIP4P-Ew, SPC/E, and TIP3P to Monatomic Anisotropic Water Models Using Relative Entropy Minimization, J. Chem. Theory Comput., 2014, 10, 4104–4120.
47. D. Nayar, M. Agarwal and C. Chakravarty, Comparison of Tetrahedral Order, Liquid State Anomalies, and Hydration Behavior of mTIP3P and TIP4P Water Models, J. Chem. Theory Comput., 2011, 7, 3354–3367.
48. B. Shadrack Jabes, D. Nayar, D. Dhabal, V. Molinero and C. Chakravarty, Water and other tetrahedral liquids: order, anomalies and solvation, J. Phys.: Condens. Matter, 2012, 24, 284116.
49. R. H. Henchman and S. J. Cockram, Water's non-tetrahedral side, Faraday Discuss., 2013, 167, 529–550.

50. D. Nayar and C. Chakravarty, Water and water-like liquids: relationships between structure, entropy and mobility, Phys. Chem. Chem. Phys., 2013, 15, 14162–14177.
51. M. S. Shell, P. G. Debenedetti and A. Z. Panagiotopoulos, Molecular structural order and anomalies in liquid silica, Phys. Rev. E: Stat., Nonlinear, Soft Matter Phys., 2002, 66, 011202.
52. D. Eisenberg and W. Kauzmann, The Structure and Properties of Water, Oxford University Press, New York, 1969.
53. H. Kitano, K. Ichikawa, M. Ide, M. Fukuda and W. Mizuno, Fourier Transform Infrared Study on the State of Water Sorbed to Poly(ethylene glycol) Films, Langmuir, 2001, 17, 1889–1895.
54. M. J. Frisch, G. W. Trucks, H. B. Schlegel, G. E. Scuseria, M. A. Robb, J. R. Cheeseman, G. Scalmani, V. Barone, G. A. Petersson, H. Nakatsuji, X. Li, M. Caricato, A. V. Marenich, J. Bloino, B. G. Janesko, R. Gomperts, B. Mennucci, H. P. Hratchian, J. V. Ortiz, A. F. Izmaylov, J. L. Sonnenberg, D. Williams-Young, F. Ding, F. Lipparini, F. Egidi, J. Goings, B. Peng, A. Petrone, T. Henderson, D. Ranasinghe, V. G. Zakrzewski, J. Gao, N. Rega, G. Zheng, W. Liang, M. Hada, M. Ehara, K. Toyota, R. Fukuda, J. Hasegawa, M. Ishida, T. Nakajima, Y. Honda, O. Kitao, H. Nakai, T. Vreven, K. Throssell, J. A. Montgomery, Jr., J. E. Peralta, F. Ogliaro, M. J. Bearpark, J. J. Heyd, E. N. Brothers, K. N. Kudin, V. N. Staroverov, T. A. Keith, R. Kobayashi, J. Normand, K. Raghavachari, A. P. Rendell, J. C. Burant, S. S. Iyengar, J. Tomasi, M. Cossi, J. M. Millam, M. Klene, C. Adamo, R. Cammi, J. W. Ochterski, R. L. Martin, K. Morokuma, O. Farkas, J. B. Foresman and D. J. Fox, Gaussian 16 Rev. C.01, 2016.
55. J. Wang, W. Wang, P. A. Kollman and D. A. Case, Automatic atom type and bond type perception in molecular mechanical calculations, J. Mol. Graphics Modell., 2006, 25, 247–260.
56. J. Wang, R. M. Wolf, J. W. Caldwell, P. A. Kollman and D. A. Case, Development and testing of a general amber force field, J. Comput. Chem., 2004, 25, 1157–1174.
57. L. B. Wright, P. M. Rodger, S. Corni and T. R. Walsh, GolPCHARMM: First-Principles Based Force Fields for the Interaction of Proteins with Au(111) and Au(100), J. Chem. Theory Comput., 2013, 9, 1616–1630.
58. S. Plimpton, Fast Parallel Algorithms for Short-Range Molecular Dynamics, J. Comput. Phys., 1995, 117, 1–19.

## 3. The effect of electric field on the structural order of water molecules around chitosan

### 3.1 Abstract

In this paper, we classified the types of water in the vicinity of the chitosan polymer and gold plate by applying an electric field of magnitude 1 V $Å^{-1}$ in various directions at varying temperatures by using molecular dynamics simulation. The three types of water were categorized by analyzing the data through the tetrahedral order method with four water regions separated in the distance from 1 to 6 Å around polymers. The interaction between water molecules and functional groups, such as hydroxyl, ether, and ester, leads to the formation of intermediate and nonfreezing water. Under an electric field, this formation appeared more clearly due to the transformation of liquid water to crystal cubic ice with two structural formations depending on gold plates at temperature 300 K. The enhancement of the tetrahedral order of water in cubic ice is related to the existence of a four-fold H-bonded structure and lower ones in the XES experiment.

### 3.2 Introduction

Water is one of the most abundant chemicals on Earth, playing a crucial role in the fluids of all known living beings. It can also be found on planets, moons, and comets.[1-2] Hydrogen bonding, molecular structure, and dipole moments of water molecules are linked across different fields, including physics, chemistry, and biology, and have a variety of industrial applications in materials science with many unique properties.[3-5] However, despite widespread interest and an enormous amount of basic and applied research, a thorough understanding of its peculiar behavior remains elusive, necessitating extensive research, particularly in superhydrophilic materials.[6-7]

The role of water molecules in the polymer interface between biological systems has been debated for a long time in determining biocompatibility of polymeric materials, especially the mechanism underlying the formation of three types of water (free water, intermediate water, and non-freezing water).[8-10] Here, its role has yet to be fully understood. In previous work[11], we successfully classified the type of water around polyrotaxane by using the tetrahedral order method.[12] This method confirmed the non-freezing water related to the ether and ester group, and the intermediate water related to the OH group in the distance from 1 to 5 Å around a polymer, by

observing four separate regions. Furthermore, the existence of a four-fold H-bonded structure and lower ones demonstrated the relationship between tetrahedral order and X-ray emission spectroscopy (XES) experiment for water.[13-14]

The current study builds on our past study on the structure and dynamics of bulk water in polymer onto a gold surface when exposed to uniform and static external electric fields in the 1 V $Å^{-1}$ range. A tiny number of water molecules were used to study the structure of water in an electric field, but the appearance of water in metal and polymer was ignored on a big scale.[15-21] In this study, the polymer observed is chitosan because it is a polycationic biopolymer composed of 2-acetamido-2-deoxy-β-D-glucopyranose and 2-amino-2-deoxy-β-D-glucopyranose residues.[22] Furthermore, the $NH_2$, ether, and ester groups, as well as OH groups in chitosan's structure are principally responsible for its properties and potential infinitive applications, especially in biomaterials and drug delivery.[23-24]

The water model TIP3P/B continues to be used due to its appropriateness for the explicit calculation of long-range electrostatic interactions. This water model can improve the description of long-range structures for a more tetrahedral HOH angle comparing TIP3P and SPCE. Furthermore, TIP3P/B accurately reflects the first peak of radial distribution function (RDF) goo and two initial troughs versus the experimental values, as well as TIP5P, a model that is reproduced perfectly with experiment goo and more properly describes the distribution of charge about the oxygen.[25] Besides, gold has been studied as a functionalized material in recent decades due to the various applications of gold nanoparticles in biological systems, such as non-toxic carriers for drug delivery, extensive surface-to-volume ratio, electrowetting, and possibilities for tailoring their charge, hydrophilicity, and functionality through surface chemistries.[26-29]

### 3.3 Results and discussion

Figures 3.1b and a show the chemical structure of chitosan polymer and the basic system configuration, which includes water, chitosan, and gold. Figures 3.1c-e depict snapshots of the final configurations of the three investigated systems (WGC, WGC-x, and WGC-z) with and without an external electric field in the x- or z-direction. On a gold plate perpendicular to the z-direction, chitosan polymer and water molecules are inserted into each system. By monitoring the physical properties of water at the

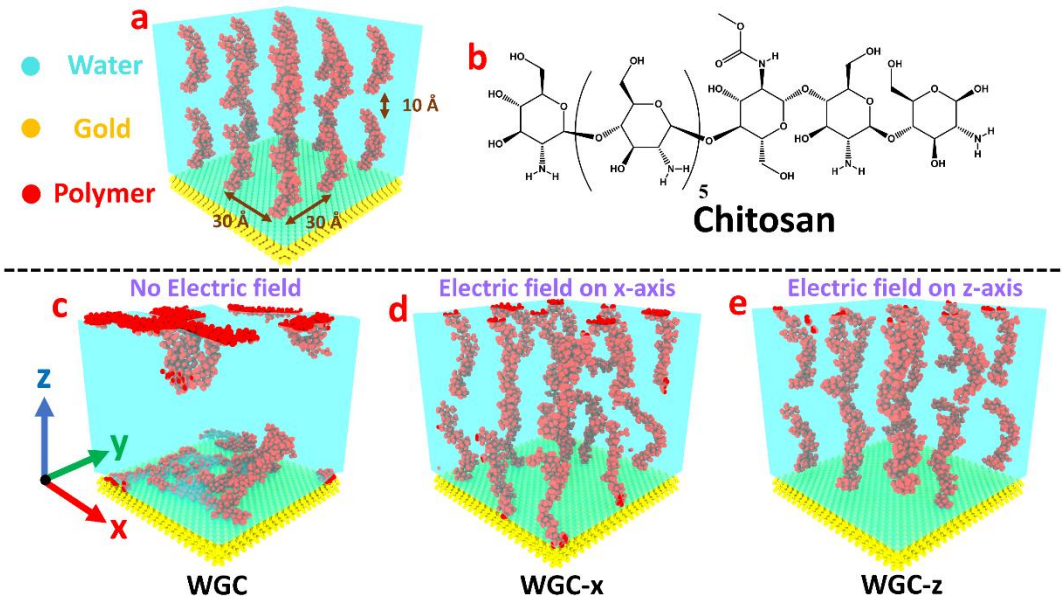


**Fig. 3.1** (a) Initial models. (b) Chemical structure of chitosan. (c-e) The snapshots of the corresponding final configurations of the three investigated systems (WGC, WGC-x, and WGC-z).

temperatures of 250 and 300 K, for simplicity, the WGC systems are named 25WGC and 30WGC, respectively (similarly to the other systems: 25WGC-x, 30WGC-x, 25WGC-z, and 30WGC-z). We also examined the properties of water at temperatures of 250 and 300 K by removing the polymer (named 25WG, 30WG, 25WG-x, 30WG-x, 25WG-z and 30WG-z). During the simulations, the gold plates are stationary, and the periodic boundary conditions are applied along the x-, y-, and z-directions. The details of the systems and the simulations are described in the Simulation section and Table 3.S1.

To observe the different structures of water with and without an electric field, we first investigated the X-ray diffraction (XRD) in systems WG, including only water and gold at temperatures 250 and 300 K. In Fig. 3.2a, the water of 30WG has an amorphous structure because it is liquid which is thermodynamically stable non-crystalline forms. Therefore, the XRD pattern is essentially continuous in appearance. However, water in 30WG-x or 30WG-z has crystallization under an external electric field in the x- or z-direction. Many sharp peaks show positions similar to planes (111), (220), (222), and (311), which belong to cubic ice (IC) structure in XRD reference ICSD 029066 and other studies.[19,30] When the temperature decreases to 250 K, the peaks of XRD patterns of 25WG-x and 25WG-z in Fig. 3.2b show

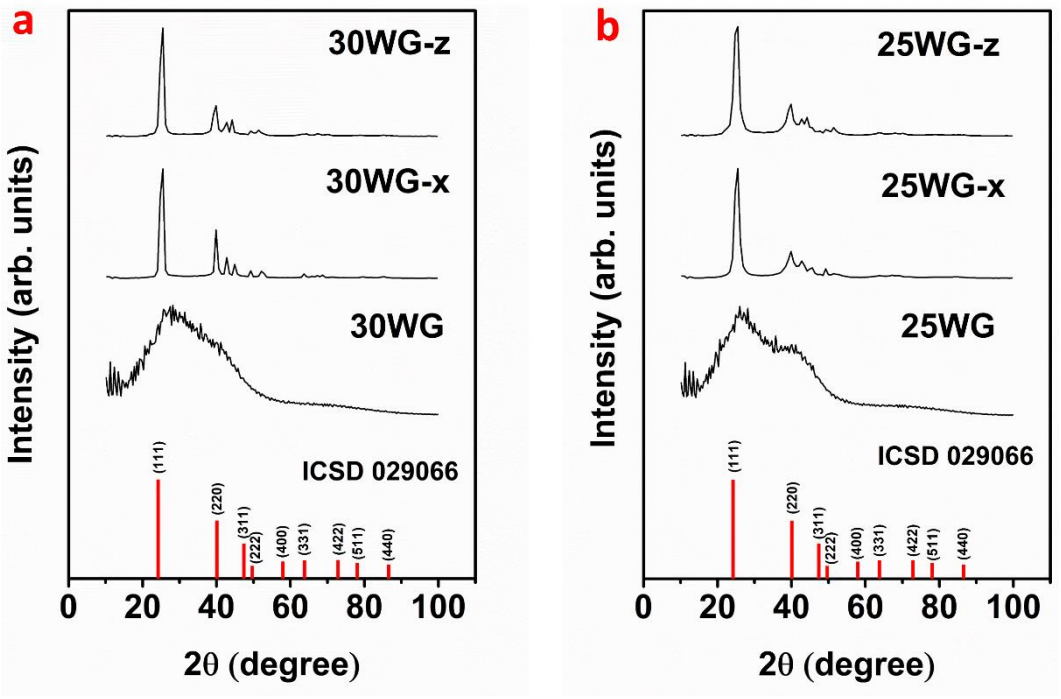


**Fig. 3.2** (a) XRD of systems 30WG, 30WG-x, and 30WG-z at temperature 300 K. (b) XRD of systems 25WG, 25WG-x, and 25WG-z at temperature 250 K.

the same positions as at the temperature of 300 K, exclusive the peaks are not sharped as them in 30WG-x and 30WG-z. It demonstrates that crystallization can occur at a high temperature in the presence of an electric field. In the system 25WG, because the TIP3P/B model is modified from TIP3P and the melting point of the TIP3P water model begins at 146 K, the structure of water remains amorphous at temperature 250 K.[31-32] Besides, we also check XRD of gold including 42 layers (Gold42) and 4 layers (Gold4) in Fig. 3.S1. Gold42 matches completely all peaks as XRD reference COD 9011612, but the peaks of Gold4 are fluctuated which peak of plane (010) is higher than plane (111).

To inspect the water distribution and the interaction between water and gold in systems WG, the density of water along the x-, y-, and z-axis was examined. In Fig. 3.3a and b, without the electric field, three layers of water appear on each side of the gold plate, which are present by three peaks: $a_1$, $b_1$, and $c_1$ along the z-axis. Due to the dominance of surface forces, similar to that reported in the literature[33-34], these forces were extensive on the hydrophilic gold surface, leading to higher peaks of water density near the gold surface. Far away from the gold surface, the water density converges

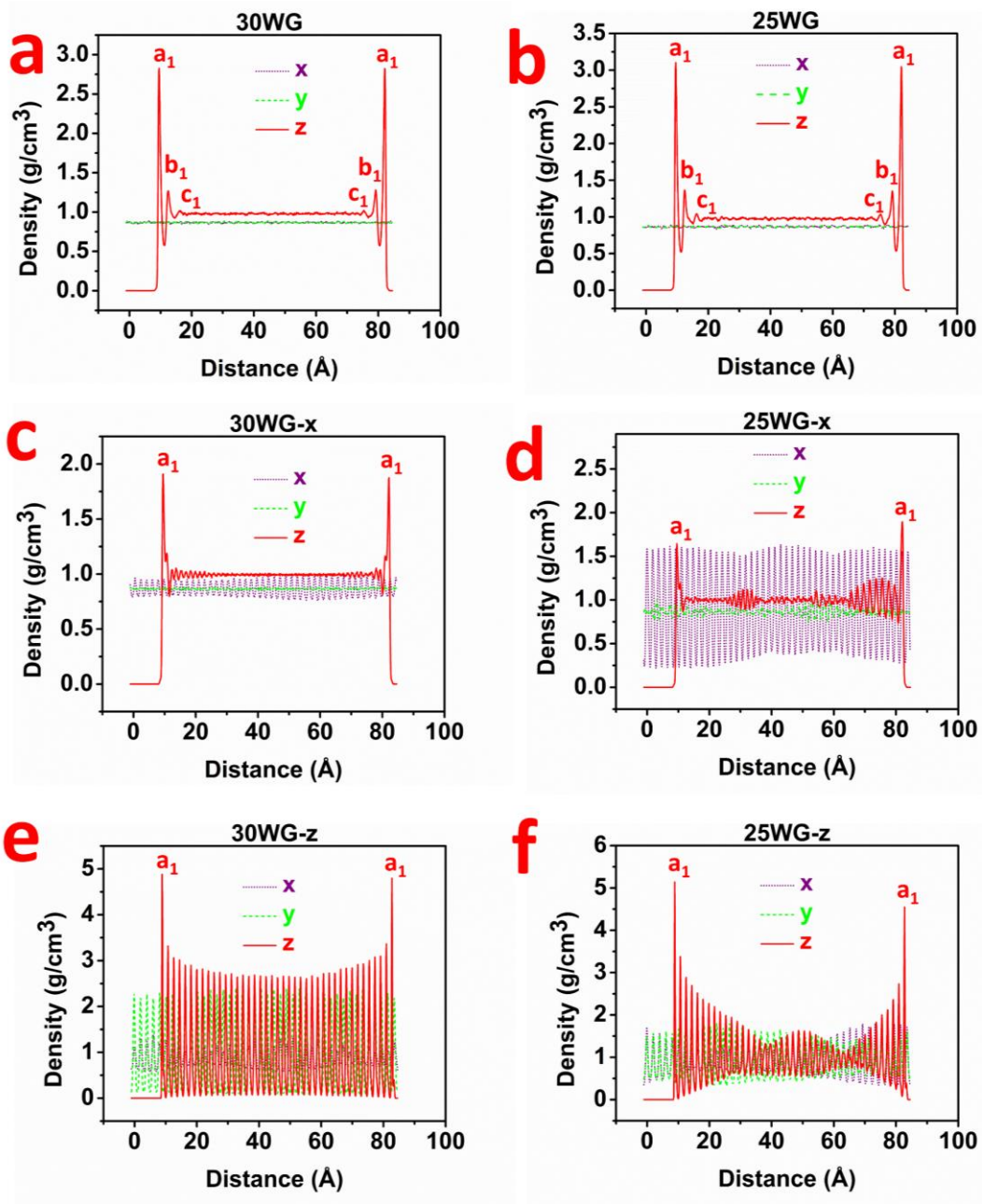


**Fig. 3.3** Density of water by x-, y-, and z-axis at 300 K and 250 K with the models (a) 30WG. (b) 25WG. (c) 30WG-x. (d) 25WG-x. (e) 30WG-z. (f) 25WG-z.

around a value of 1 g $cm^{-3}$. The zero-density region between the liquid and solid surfaces has been observed experimentally and mathematically.[35-36] The water density on the x-axis and y-axis are horizontal lines with an approximated value of 0.87 g $cm^{-3}$ due to the absence of gold plates on these axes.

With an electric field along the x-direction, the water density of 30WG-x

on the z-axis displays the highest peak $a_1$ and several low peaks oscillating, gradually reducing to 1 g $cm^{-3}$ in Fig. 3.3c instead of only three peaks in system 30WG or 25WG on each gold surface. On the x-axis, the water density of 30WG-x exhibits the waves with oscillation amplitudes ranging from 0.76 to 1 g $cm^{-3}$, but on the y-axis, the water density remains a horizontal line. It suggests that under an electric field along the x-direction, water molecules interact to form many parallel layers on the x-axis. This phenomenon is known as water whiskers, and it occurs when water aggregates become linear and long chains of water form under high electric fields.[15] When the temperature decreases to 250 K, the water density of 25WG-x on the x-axis reveals water whiskers more clearly with oscillation amplitudes of waves ranging from 0.21 to 1.64 g $cm^{-3}$ in Fig. 3.3d. However, the water density of 25WG-x on the z-axis, except for the highest peak $a_1$, exposes many areas of randomly low peaks, which do not converge gradually to 1 g $cm^{-3}$ as results in systems 30WG and 25WG. On the y-axis, the water density of 25WG-x produces similar results as on the z-axis except for the absence of the highest peak $a_1$. The difference in water density between 30WG-x and 25WG-x is due to temperature variations. The water molecules at 250 K travel more slowly than those at 300 K. Furthermore, the electric field in the x-direction affects the water molecules to create water whiskers; meanwhile, two hydrogen and two lone pairs of valence electrons on the atom oxygen of a water molecule connect easily with four other water molecules to form a tetrahedral arrangement.[1,37] As a result, the water density of 25WG-x looks to be almost separated layers on the x-axis when compared to 30WG-x, but the water molecules of 25WG-x require a longer time on the z-axis and y-axis to achieve the same results as 30WG-x.

With an electric field along the z-direction, the water density of 30WG-z on the z-axis, which forms by the water whiskers, appears not only in the quite uniform peaks with oscillation amplitudes of waves ranging from 0.01 to 3.72 g $cm^{-3}$ but also in the highest peak $a_1$ on each gold surface in Fig. 3.3e. On the y-axis, the water density of 30WG-z shows rather homogeneous peaks with oscillation amplitudes of waves ranging from 0.09 to 2.41 g $cm^{-3}$, whereas the peaks on the x-axis fluctuate erratically with oscillation amplitudes of waves ranging from 0.57 to 1.38 g $cm^{-3}$. The water densities on the x-, y-, and z-axes for system 25WG-z are similar to the water density of 30WG-z on the x-axis. It verifies the XRD findings above

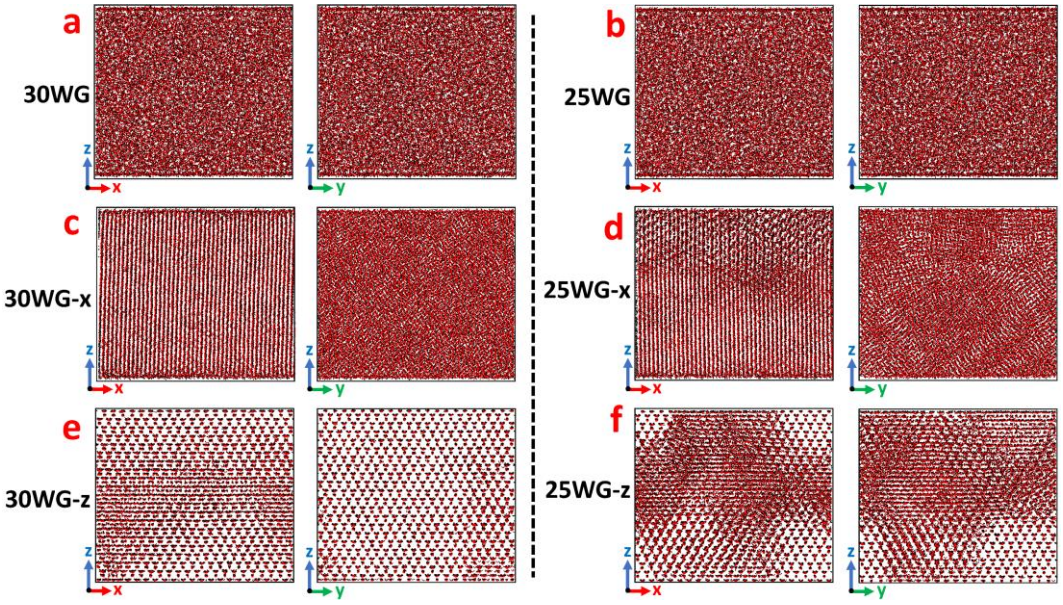


**Fig. 3.4** The snapshots of the corresponding final configurations of the three investigated systems (WG, WG-x, and WG-z) in planes xz and yz at temperatures 250 and 300 K. (a) 30WG. (b) 25WG. (c) 30WG-x. (d) 25WG-x. (e) 30WG-z. (f) 25WG-z.

that water crystallizes faster at 300 K than at 250 K under an electric field, especially in the z-direction, where gold plates are put on the z-axis.

Fig. 3.4 shows snapshots of the final configurations of the six systems for visual views of the parallel layers (water whiskers) in water density and structure (30WG, 30WG-x, 30WG-z, 25WG, 25WG-x, and 25WG-z). In the absence of an electric field, water molecules in systems 30WG and 25WG are arranged in perturbation, regardless of whether the temperature is 300 K or 250 K in Fig. 3.4a and b. In the presence of an electric field along the x-axis, water molecules in systems 30WG-x and 25WG-x produce parallel layers, but the parallel water layers in 25WG-x are more perpendicular to the x-axis than those in 30WG-x in Fig 3.4c and d. It explains why the water density of 25WG-x on the x-axis produces waves with oscillation amplitudes greater than those of 30WG-x in Fig. 3.3c and d. The most intriguing aspect is that water molecules in system 30WG-z are organized diamond-type tetragonal structures of an ordered version of ice IC with an electric field applied perpendicularly on gold plates in Fig. 3.4e. However, this crystallization requires an external electric field and a below temperature of 190 K to get a stable structure, according to prior research by our colleagues.[38-42] Therefore, our models are simple and easy to obtain

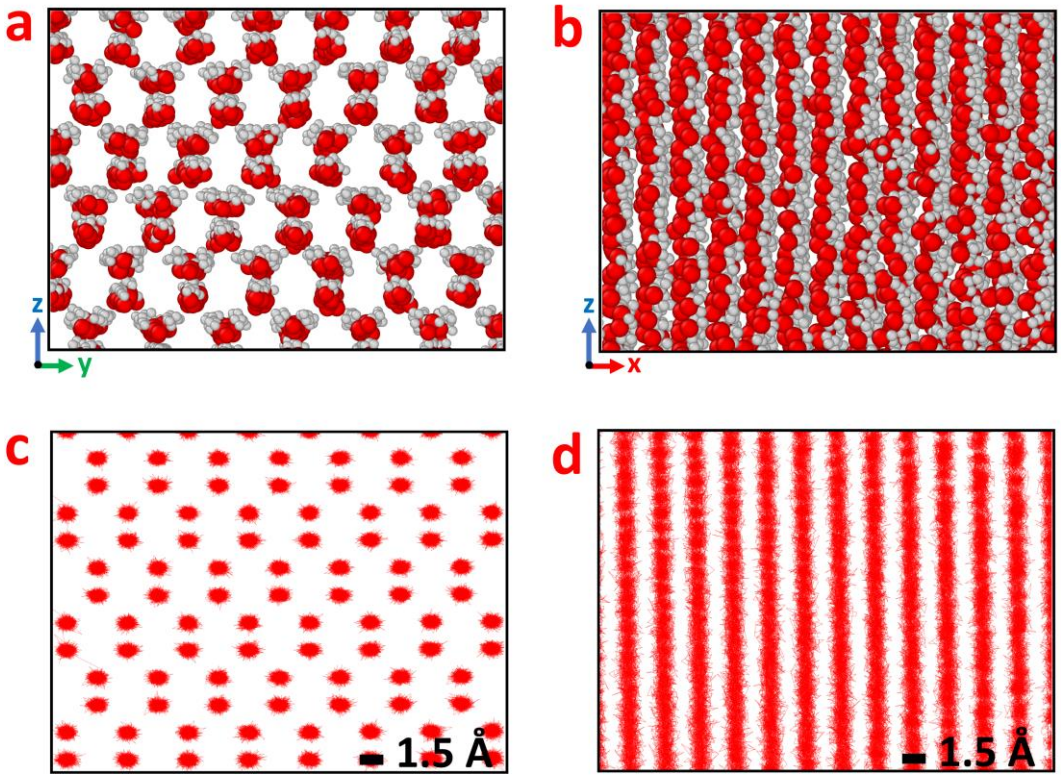


**Fig. 3.5** The water structures and trajectories of oxygen in water molecules traveling during 0.5 ns are zoomed-in. (a) Diamond-type tetragonal structures. (b) Water whiskers structures. (c) Trajectories of diamond-type tetragonal structures. (d) Trajectories of water whiskers

this ice structure at room temperature. In Fig. 3.4f, at 250 K, the water molecules of 25WG-z display the mixture of water whiskers and tetragonal structures. It indicates that the water whiskers are transformed into diamond-type tetragonal formations during the process.

For a clearer view, in Fig. 3.5c and a, the trajectories of oxygen atoms in water molecules traveling during 0.5 ns are also drawn, and the water structures are zoomed-in for the diamond-type tetragonal structures, respectively. The molecular dipoles in this crystal's lattices all point in the same direction along the z-axis due to the appearing electric field in z-direction. Furthermore, the trajectories reveal that oxygen atoms move around within a diameter of 1.5 Å in fixed positions. With the electric field in the x-direction, in Fig. 3.5b and d, the molecular dipoles of water whiskers structures are all oriented in the same direction along the x-axis, and the trajectories show that the water molecules of each water whisker layer only travel on this layer. There is no interference between water

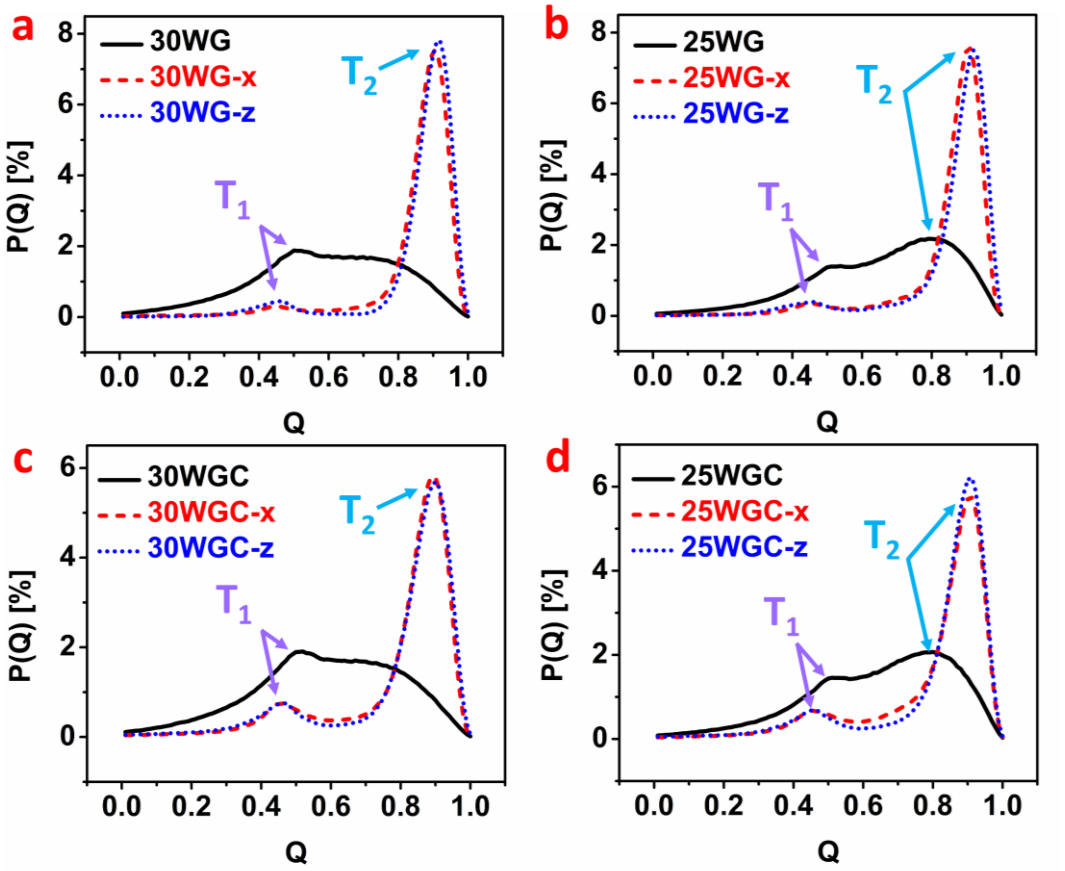


**Fig. 3.6** Orientational tetrahedral order of oxygen water at 250 and 300 K. (a) 30WG, 30WG-x, and 30WG-z. (b) 25WG, 25WG-x, and 25WG-z. (c) 30WGC, 30WGC-, and 30WGC-z. (d) 25WGC, 25WGC-x, and 25WGC-z.

whisker layers, and the width for each layer is 1.36 Å. As a result, when an electric field is applied, diamond-type tetragonal and water whiskers structures are extremely stable.

In the next survey, we examined at the tetrahedral order of oxygen in water molecules and polymers to better understand diamond-type tetragonal structures and classify water around the polymer. The orientational order parameter q for 4-coordinated water molecules has been thoroughly addressed by Debenedetti and Errington.[12] The following formula calculates the local tetrahedral associated with a particular oxygen atom i:

$$q_{tet} = 1 - \frac{3}{8}\sum_{j=1}^{3}\sum_{k=j+1}^{4}\left(\cos\theta_{ijk} + \frac{1}{3}\right)^2 \quad (1)$$

where θ is the angle between the bond vectors $r_{ij}$ and $r_{ik}$, and the j and k labels are typical for the four nearest oxygen atoms. This formula is the most

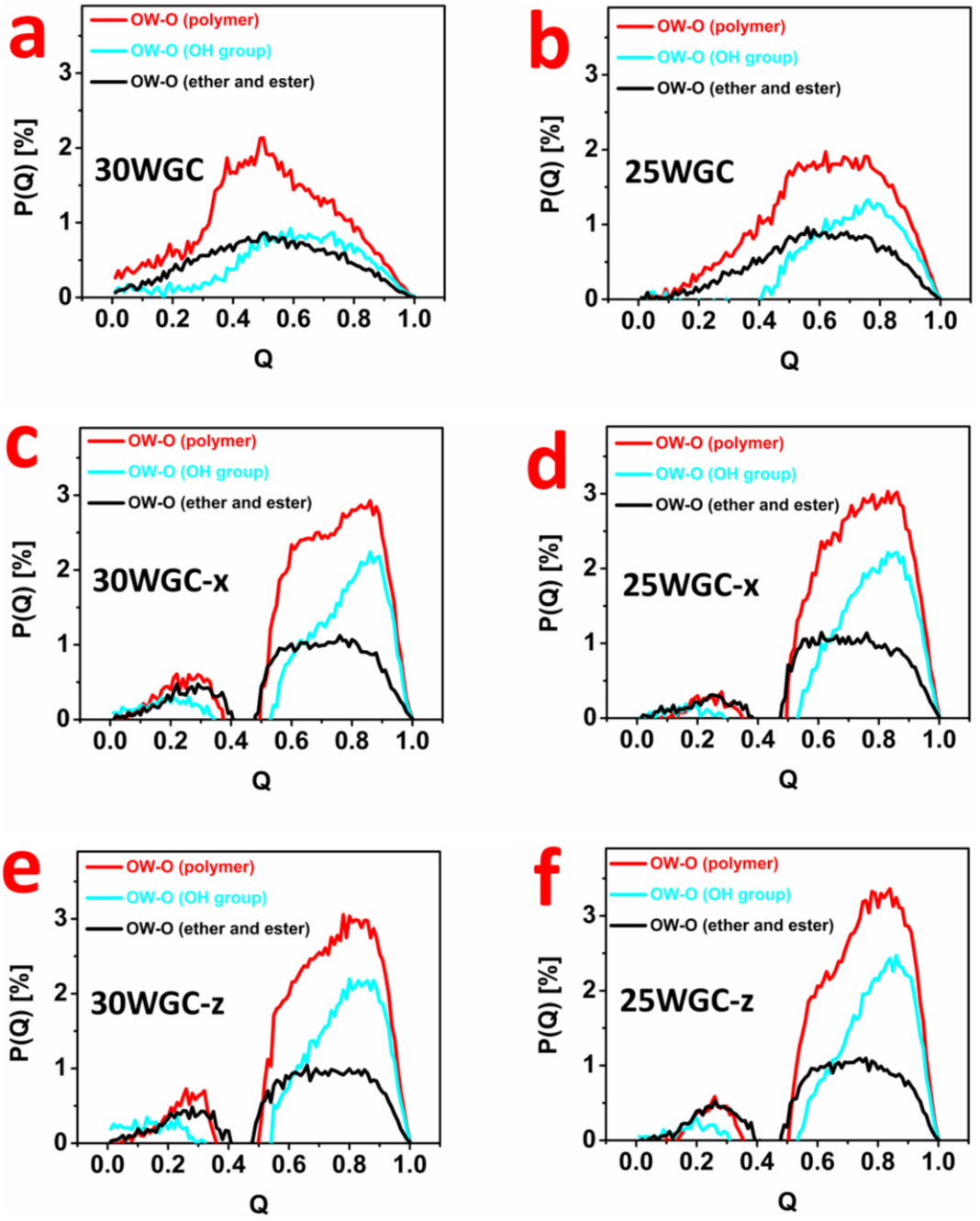


**Fig. 3.7** Orientational tetrahedral order at 300 and 250 K by oxygen in water with total oxygen of polymer (red curve), oxygen in water with oxygen in OH group (cyan curve) and oxygen in water with oxygen in ether and ester group (black curve). Red curve = cyan curve + black curve.

common type for tetrahedral order parameters.[43-47] The four closest oxygen neighbors in the water molecules and polymer are used to compute this order parameter. The value of q can range from 0 to 1, with 0 being the ideal

gas/the disorder and 1 representing the perfect tetrahedral structure/the order.

In Fig. 3.6, we checked the tetrahedral order of the oxygen atoms of water for all the models. At 300 K, system 30WG has one prominent peak named $T_1$ at q = 0.5 with P(Q) = 1.87 in Fig. 3.6a. Nevertheless, under the electric field, the peaks $T_1$ of systems 30WG-x and 30WG-z shift slightly on the left at values q = 0.45 and 0.46, with reducing the intensities P(Q) = 0.29 and 0.45, respectively. Furthermore, the sharp peaks $T_2$ appear at q = 0.9 and 0.92 in systems 30WG-x and 30WG-z, respectively, with a high-intensity P(Q) of nearly 8. Therefore, under the influence of an electric field, water molecules easily acquire the order or tetrahedral formations. In comparison to 30WG, 30WG-x, and 30WG-z, the peaks $T_1$ emerge clearer and the peaks $T_2$ fall lower for the intensities P(Q) with systems 30WGC, 30WGC-x, and 30WGC-z in Fig. 3.6c. It suggests that chitosan polymers interact with water molecules, causing the disorder to increase. At 250 K, except for 25WG and 25WGC, the graphs of systems 25WG-x, 25WG-z, 25WGC-x, and 25WGC-z in Fig. 3.6b and d show the same features as systems at 300 K. In contrast to the sharp and high intensity of peaks $T_2$ in systems 25WG-x and 25WG-z, the peak $T_2$ arises in systems 25WG and 25WGC with a round form and low intensity P(Q). It indicates that when the temperature drops, the tetrahedral structures in water grow. This rise, however, is not as significant as water in an electric field.

To assess the affinity of the ether and ester group and OH group to the structure of water, we continued to study the tetrahedral order of oxygen, including the oxygen of polymer and oxygen of water around the polymer (Fig. 3.7). The polymer has 702 oxygen atoms, with 360 in the OH group and 342 in the ether and ester groups. We examined the tetrahedral order not only for the total amount of oxygen atoms of the polymer (red curve) with the oxygen atoms of water but also for the oxygen in the ether and ester groups (black curve) or the oxygen in the OH group (cyan curve) with the oxygen atoms of water. The red curve represents the summation of the cyan and black curves. Without the electric field, at temperature 300 K, the red and black curves in system 30WGC have the peaks $T_1$ around q = 0.5, and the shape of the black curve is relatively symmetric, except the red and cyan curves tend to asymmetry with the area under the curve at $q \geq 0.5$ larger than $q < 0.5$ as shown in Fig. 3.7a. However, at temperature 250 K, the red, cyan, and black curves in system 25WGC tend to asymmetry, with the area under the curve at $q \geq 0.5$ larger than $q < 0.5$ in Fig. 3.7b. Therefore, the OH groups

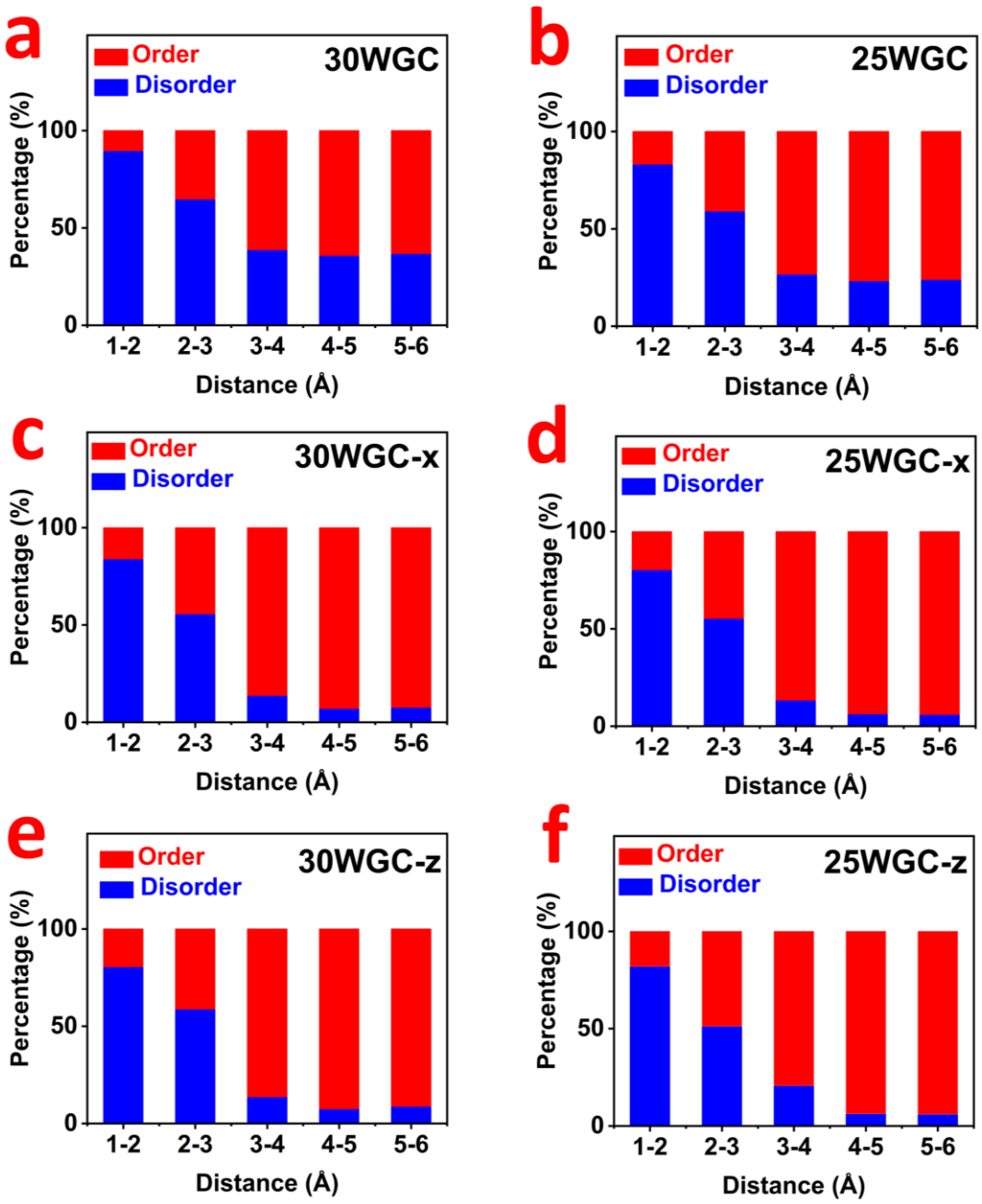


**Fig. 3.8** The percentage (%) of oxygen waters which reside in order and disorder by shortest distance to chitosan polymers at 300 K for models (a) 30WGC. (c) 30WGC-x. (e) 30WGC-z; and 250 K for models (b) 25WGC. (d) 25WGC-x. (f) 25WGC-z.

increase the tetrahedral structure/the order of water molecules despite temperature 300 K or 250 K. Meanwhile, the ether and ester groups contribute a half order and a half disorder at 300 K, but offer more order than disorder at 250 K. These results confirm our previous study and other

scientists' studies that the hydrogen bond interactions of ether and ester groups with water, such as C–O···HOH···HOH and C–O···HOH were related to intermediate water, whereas C=O···HOH, C=O···HOH···O=C, and C–O···HOH···O–C were associated to non-freeze water.[8,48] The hydrogen bond interactions of OH groups with water such as C– OH···HOH, C–OH···HOH···O–C, and HOH···OH···HOH can be considered to the formation of intermediate water.[49] Here, because non-freezing water does not freeze below 273 K, it lacks structures and is classified as the disorder. On the other hand, the intermediate water is freezable below 273 K and hence has a tetrahedral structure, making it the order.

With the appearing electric field, the graphs of the tetrahedral order parameter in Fig 3.7c-f are split by two specific regions, identical to the two peaks $T_1$ and $T_2$ in Fig. 3.6. The section beginning at q from 0.5 to 1 is referred to as the ordered region, while the section beginning at q from 0.4 to 0 is referred to as the disordered region. The ordered regions have larger areas and higher probability P(Q) values than the disordered regions. In addition, the red curves of ordered regions have shoulder peaks compared to broad peaks of the cyan curve due to the continuous appearance of the black curve, and the height of black curves is also lower than those of cyan curves. In contrast, in the disordered regions, the area and height of black curves are larger and higher than cyan curves. As a result, an electric field in the x or z direction increases the number of tetrahedral structures of water, but the number of tetrahedral structures of water in polymers increases or decreases depending on whether the ratio of ether and ester groups and OH groups in polymers is lower or higher than 1.

Based on the results in Fig. 3.6 and 3.7, we categorized the water molecules belonging to $q \geq 0.5$, were classified as the order, while others were the disorder with $q < 0.5$. Hence, water was classified based on the shortest distance from its oxygen atoms to the polymer atoms (Fig. 3.8). Therefore, we focused on water molecules around the polymer from 0 to 6 Å to study the width and distance of each type of water around the polymer. Here, the last frame in the equilibrium simulation of twelve relaxation nanoseconds was considered for the calculations. There are no water molecules in the distance from 0 to 1 Å. For all systems, the percentages of water molecules belonging to the disorder are more dominant than those belonging to the order when the distance is between 1 and 2 Å with

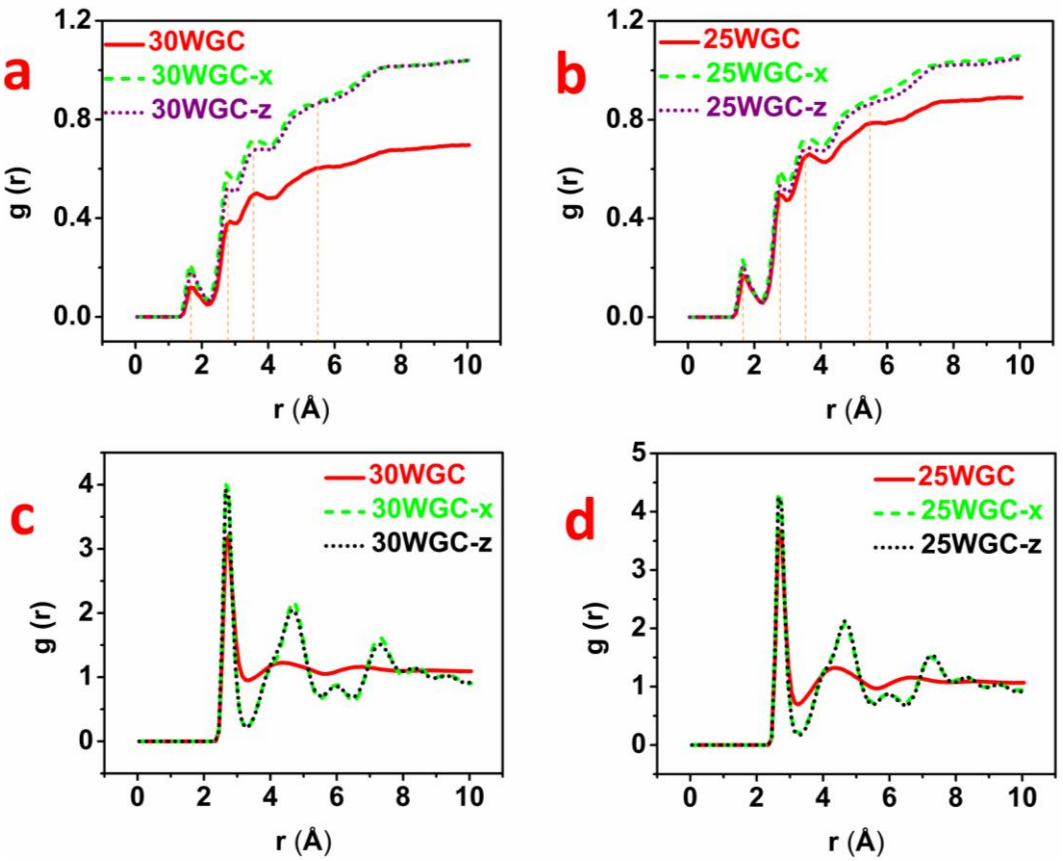


**Fig. 3.9** (a) and (b) Radial distribution function (RDF) between the oxygen of water molecules and atoms of polymers. (c) and (d) RDF of oxygen water.

percentages greater than 80%. As a result, the first zone should have non-freezing water.

Despite the reduction in temperature from 300 to 250 K and the appearance of an electric field in the x or z direction, the percentages of disorder fall in the distance from 2 to 3 Å, but the values are still over 50% when compared to those of order. Therefore, the second zone is an interference area of non-freezing and intermediate water with a distance of 2 to 3 Å. In the distance from 3 to 6 Å, the percentages of order outrace to compare those of disorder for all systems with values above 80% except 30WG with values above 61% and 25WG with values above 73%. However, in Fig. 3.8c-f, when an electric field appears in the x or z direction, the percentages of order in the distance from 4 to 6 Å are higher than those in the distance from 3 to 4 Å with values greater than 90%. Consequently, the third zone should be intermediate water with a distance from 3 to 4 Å. The fourth zone is an interference area of intermediate water and free water in the distance from 4 to 5 Å because its

number of water molecules is lower than that of in the distance from 5 to 6 Å (Fig. 3.S2). Water molecules are related to free water if the distance between them and polymers is higher than 5 Å.

For verification of tetrahedral order method by experiment, in our previous study[11], we showed the relationship between tetrahedral order parameter and XES experiment, by comparing two peaks $T_2$ (tetrahedral order) and $T_1$ (disorder) to two peaks $1b_1$' (four-fold H-bonded structure) and $1b_1$'' (less than four-fold), respectively. In this study, at temperatures below 273K, the peaks $T_2$ and $T_1$ of systems 25WG and 25WGC are similar to the peaks $1b_1$' and $1b_1$'' of crystalline ice, respectively.[13,14,50-52] Furthermore, due to the separation completely of two peaks $T_2$ and $T_1$ with the appearance of the electric field in Fig. 3.6 and Fig. 3.7c-f despite the temperature, we suggest including the electric field in the XES experiment in order to see two peaks $1b_1$' and $1b_1$'' of water in polymer more clearly. By combining tetrahedral order in simulation and XES to compare with other known methods, we may better understand the development of water types surrounding polymers.

The distribution of the water molecules around the polymer using RDF between the oxygen atoms of water and the atoms of the polymer is plotted in Fig. 3.9a and b. Again, there are no water molecules at a distance of 0 to 1 Å measured from any atom of the polymer; thus, no hydrogen bond exists between water and the polymer. We identified three distinct peaks in the distance of 1 to 4 Å despite temperatures of 300 or 250 K and with or without an electric field. However, in the distance of 5 to 6 Å, the fourth peak is broad, so the fourth region is thinner than the other three regions. For the further distances, there are no peaks and no interaction between polymer and water. Figure 3.9c and d show the oxygen-oxygen RDF of water for all WGC systems at temperatures of 250 and 300 K, including with and without an electric field. Without the electric field, the g(r) of water in systems 30WGC and 25WGC shows the greatest peak at r = 2.75 Å and multiple low and broad peaks oscillating, progressively dropping the density to 1 g $cm^{-3}$. The peaks in systems 30WGC-x, 30WGC-z, 25WGC-x, and 25WGC-z show g(r) values higher than those in systems 30WGC and 25WGC when an electric field is applied in the x or z directions. These wave fluctuations, on the other hand, are unable to converge the density to 1 g $cm^{-3}$ as quickly as those without an electric field and matches the data reported in.[39]

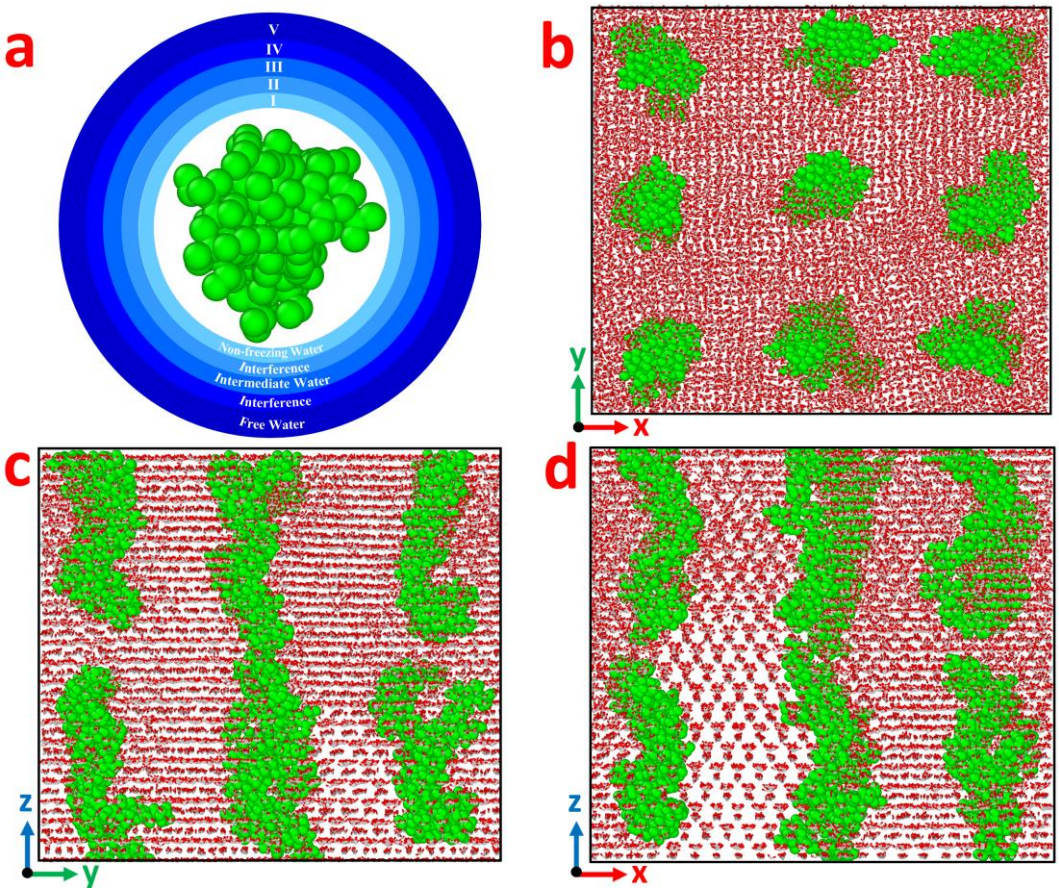


**Fig. 3.10** (a) The illustration of four water layers around polymer. (b-d) The snapshots of the corresponding final configurations of 30WGC-z.

We also calculate the radius of gyration $R_g$ of the atoms of chitosan polymers, including all effects due to atoms passing through periodic boundaries. $R_g$ is a measure of the size of the group of atoms, and is defined as the square root of the $R_g^2$ value in this formula[53]:

$$R_g{}^2 = \frac{1}{M}\sum_i m_i(r_i - r_{cm})^2 \qquad (2)$$

where M is the total mass of the group, $r_{cm}$ is the center-of-mass position of the group, and the sum is over all atoms in the group. The value $R_g$ of polymers in the initial configurations is 40.9. In the absence of an electric field, the values $R_g$ in systems 30WGC and 25WGC are 52.1 and 48.5, respectively, once the simulations reach equilibrium. The values $R_g$ in systems 30WGC-x, 30WGC-z, 25WGC-x, and 25WGC-z, on the other hand, do not vary significantly as the electric field appears, with values of 42.8, 42.3, 41.9, and 41.7, respectively. It means that the electric field maintains the shape of polymers, and that high temperatures enhance $R_g$ in comparison

to low temperatures; thus, it increases the interaction between water molecules and functional groups in polymers. For a clearer view, the configurations of polymers are zoomed-in in Fig. 3.S3.

**Simulation Section**

Each simulation box with a size of x × y × z = 86 × 86 × 86 $Å^3$ contains eighteen chitosan polymers and 18225 water molecules and one Au plate (Fig. 3.1). The Au plate of 3528 atoms has the sizes in the x- and y-directions equal to those of the box and the four atomic layers in the z-direction. One chitosan polymer is described in detail in Fig. 3.1, includes one 2-acetamido-2-deoxy-β-D-glucopyranose and eight 2-amino-2-deoxy-β-D-glucopyranose monomers. In the initial configurations, the water molecules are regularly arranged along the directions with constant distances of (x, y, z) = (3.1, 3.1, 3.1) Å. General AMBER Force Field (GAFF) parameters are used to describe the interactions between the atoms of the chitosan polymer which were calculated from AM1-BCC by Antechamber.[54-55] GolPCHARMM parameters for the interactions of Au–Au were taken from the literature.[26] Lorentz–Berthelot rules are used to calculate the interaction parameters between two unrelated non-bonded atoms. Long-range Coulombic interactions are computed in particle–particle–particle-mesh (pppm) K-space. All atomistic simulations were performed with the LAMMPS package.[56] Each system is under NVT canonical ensemble behavior and periodic boundary conditions in the x-, y- and z-directions. The atoms of the Au plates are fixed during the simulations. Temperature is controlled by the Nose–Hoover thermostat method. The uniform and static external electric field in the 1 V $Å^{-1}$ range is applied in the x- or z-direction. Properties of each system are detected at the two different temperatures of 250 and 300 K for comparison. The equations of motion are integrated using the velocity-Verlet algorithm with a time step of 1 fs. Each WG and WGC simulation are run in the time of 8 and 12 ns, respectively, and the obtained values are averaged over this time. After 8 and 12 ns, the simulations achieve equilibrium by temperature, total energy, and the radius of gyration of the polymer.

## 3.4 Conclusions

In conclusion, the electric field increases the tetrahedral arrangement of water leading to the formation of water whiskers with the structure similar to the cubic ice. These water whiskers are transformed into diamond-type

tetragonal formations when water molecules inserted between the Au plates, and the electric field is set perpendicular to Au plates. Under the strong electric fields with 1 V $Å^{-1}$, we also have shown that our simulation study successfully distinguishes non-freezing water and intermediate water based on an investigation of the tetrahedral order of water molecules around a polymer at distances ranging from 1 to 6 Å by seeing four distinct zones. For visualization, Fig. 3.10 shows the illustration of four distinct water zones around polymer and the snapshots of the corresponding final configurations of 30WGC-z. The first zone is non-freezing water and is the nearest from the polymer. The second zone is an interference area of non-freezing water and intermediate water. The third zone is made up of intermediate water. The fourth zone, which is the narrowest, is an interference area of intermediate and free water caused by the polymer and water's weak interaction. Water molecules are considered free water after a distance of 6 Å.

### 3.5 Support Information

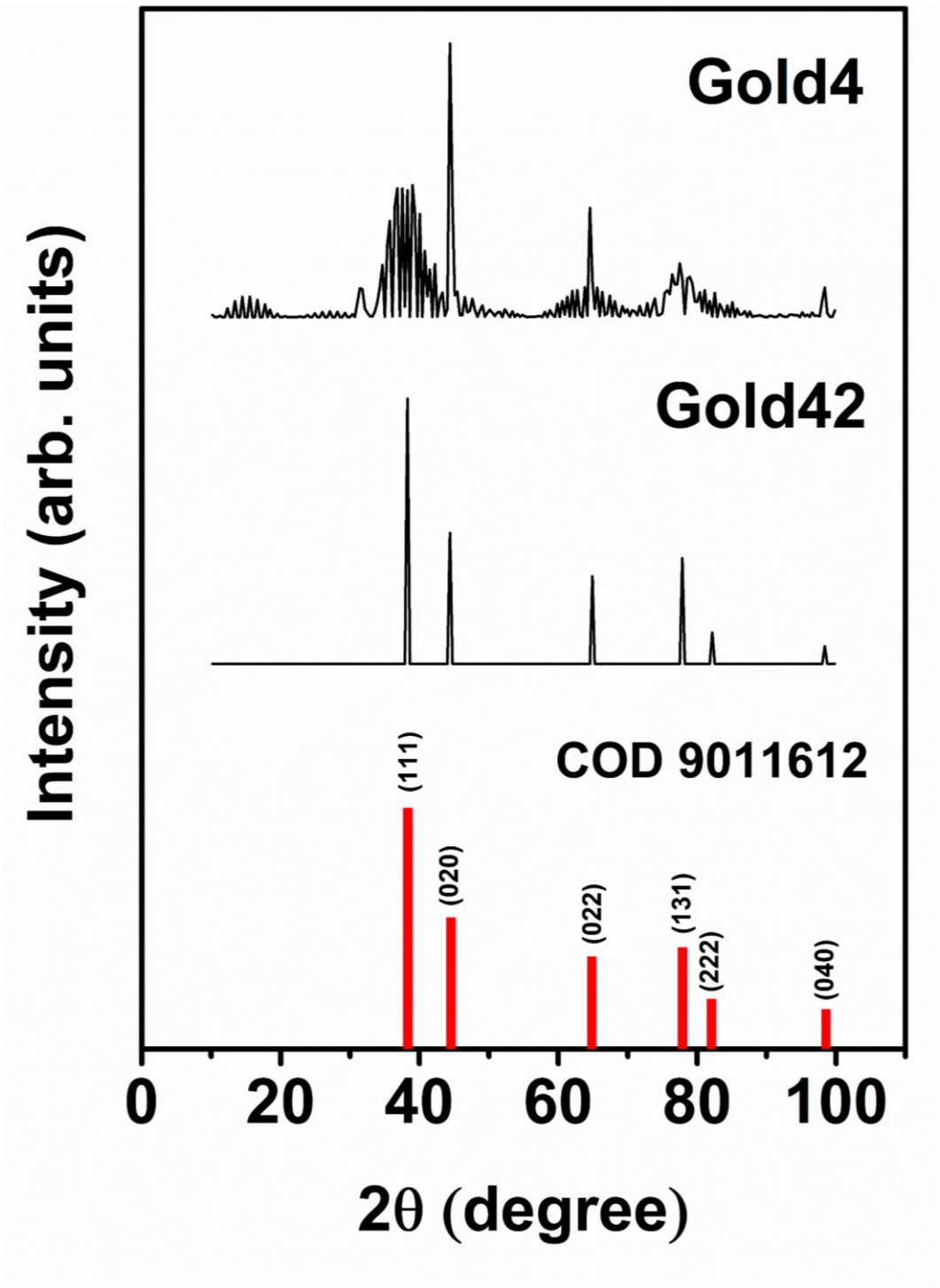


**Fig. 3.S1** XRD of gold plates with Gold42 including 42 layers and Gold4 including 4 layers.

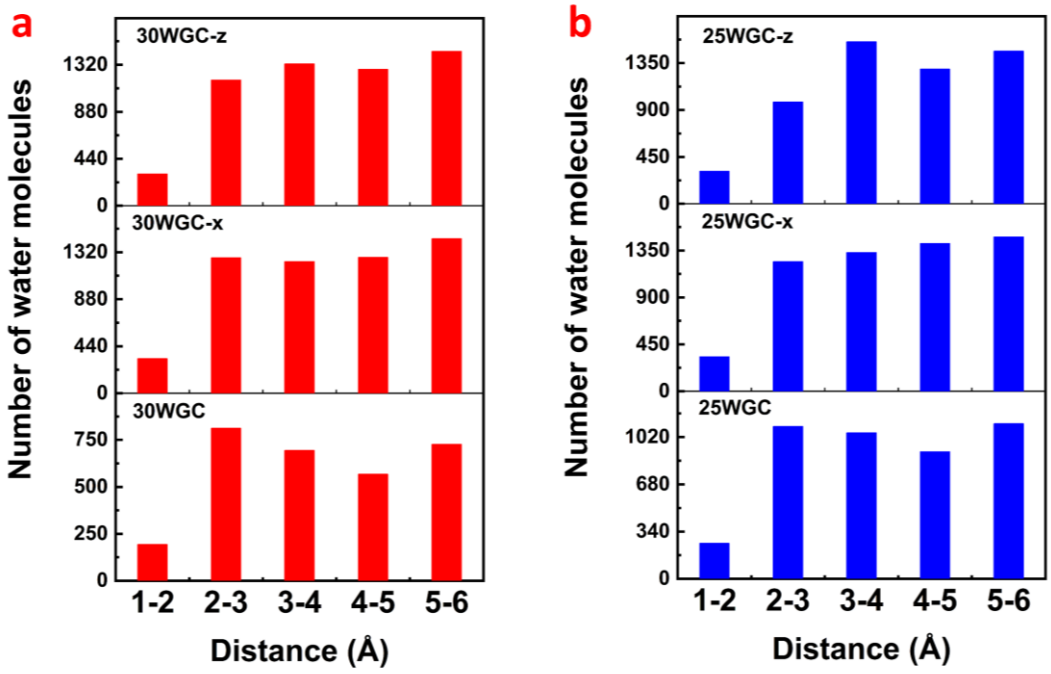


**Fig. 3.S2** Number of water molecules around polymers by the shortest distance of oxygen water to chitosan at 300 K and 250 K in systems including WGC, WGC-x, and WGC-z.

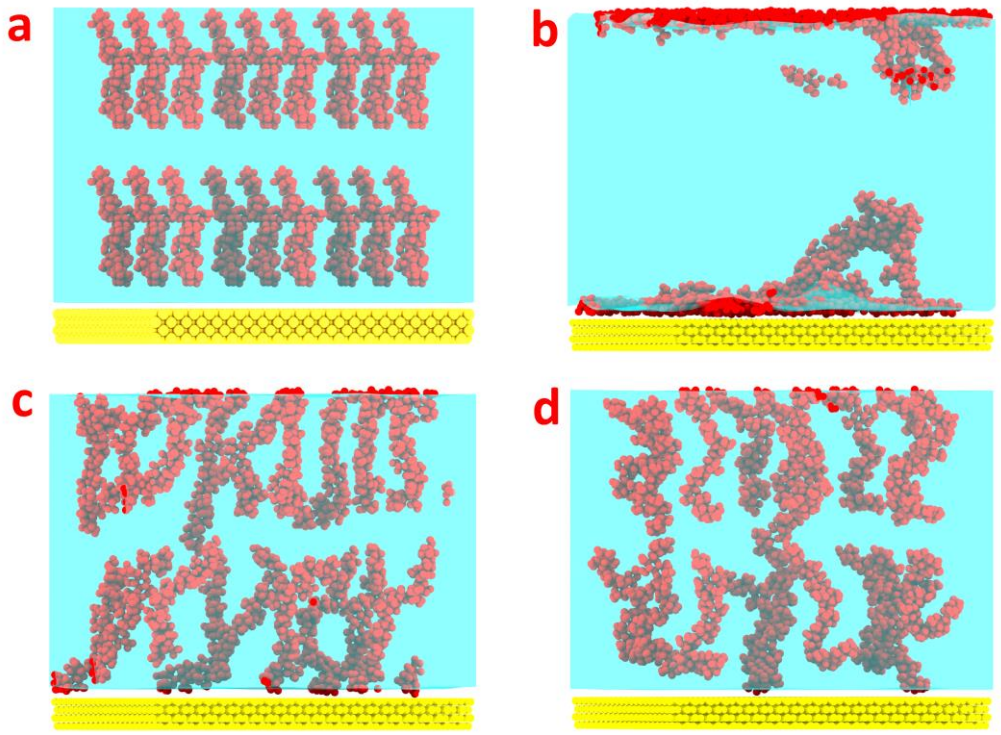


**Fig. 3.S3** Snapshots of configurations including 18 chitosan polymers. (a) The initial configurations. (b) The final configurations without the electric field. (c) and (d) The final configurations with the appearing electric field in x- and z-direction, respectively.

**Table 3.S1.** System specifics of all models.

| Name System | Number of polymers | Water molecules | Gold atoms | Temperature | Electric Field |
|---|---|---|---|---|---|
| **30WG** | None | 18,225 | 3,528 | 300 K | None |
| **30WG-x** | None | 18,225 | 3,528 | 300 K | x-direction |
| **30WG-z** | None | 18,225 | 3,528 | 300 K | z-direction |
| **25WG** | None | 18,225 | 3,528 | 250 K | None |
| **25WG-x** | None | 18,225 | 3,528 | 250 K | x-direction |
| **25WG-z** | None | 18,225 | 3,528 | 250 K | z-direction |
| **30WGC** | 18 | 18,225 | 3,528 | 300 K | None |
| **30WGC-x** | 18 | 18,225 | 3,528 | 300 K | x-direction |
| **30WGC-z** | 18 | 18,225 | 3,528 | 300 K | z-direction |
| **25WGC** | 18 | 18,225 | 3,528 | 250 K | None |
| **25WGC-x** | 18 | 18,225 | 3,528 | 250 K | x-direction |
| **25WGC-z** | 18 | 18,225 | 3,528 | 250 K | z-direction |

**Table 3.S2.** The averaged atomic partial charges of chitosan were calculated from AM1-BCC by Antechamber.

| Types of atom | Charge |
|---|---|
| c | 0.7251 |
| c3 | 0.1432 |
| h1 | 0.0762 |
| h2 | 0.0779 |
| hn | 0.3631 |
| ho | 0.4203 |
| n | -0.4849 |
| n3 | -0.9084 |
| o | -0.601 |
| oh | -0.5996 |
| os | -0.4379 |

**References**


1 P. Ball, H2O: A Biography of Water, Phoenix2000.

2 J. P. Poirier, Nature, 1982, 299, 683-687.

3 A. Ben-Naim, Molecular Theory of Water and Aqueous Solutions.

4 K. Sato, S. Kobayashi, M. Kusakari, S. Watahiki, M. Oikawa, T. Hoshiba and M. Tanaka, Macromolecular Bioscience, 2015, 15, 1296-1303.

5 Y. Ishii, N. Matubayasi and H. Washizu, The Journal of Physical Chemistry B, 2022, 126, 4611-4622.

6 P. Ball, Chemical Reviews, 2008, 108, 74-108.

7 M. A. Bag and L. M. Valenzuela, Int J Mol Sci, 2017, 18.

8 T. Tsuruta, Journal of biomaterials science. Polymer edition, 2010, 21, 1831-1848.

9 M. Tanaka and A. Mochizuki, Journal of Biomedical Materials Research Part A, 2004, 68A, 684-695.

10 A.-T. Kuo, S. Urata, R. Koguchi, K. Yamamoto and M. Tanaka, Polymer, 2019, 170, 76-84.

11 T. M. N. Le, L. Van Sang and H. Washizu, Physical Chemistry Chemical Physics, 2022, 24, 2176-2184.

12 J. R. Errington and P. G. Debenedetti, Nature, 2001, 409, 318-321.

13 E. Gilberg, M. J. Hanus and B. Foltz, The Journal of Chemical Physics, 1982, 76, 5093-5097.

14 T. Tokushima, Y. Harada, O. Takahashi, Y. Senba, H. Ohashi, L. G. M. Pettersson, A. Nilsson and S. Shin, Chemical Physics Letters, 2008, 460, 387-400.

15 M. Karahka and H. J. Kreuzer, Physical Chemistry Chemical Physics, 2011, 13, 11027-11033.

16 A. T. Celebi, M. Barisik and A. Beskok, The Journal of Chemical Physics, 2017, 147, 164311.

17 A. M. Saitta, F. Saija and P. V. Giaquinta, Physical Review Letters, 2012, 108, 207801.

18 L. B. Skinner, C. J. Benmore, B. Shyam, J. K. R. Weber and J. B. Parise, Proceedings of the National Academy of Sciences, 2012, 109, 16463-16468.

19 T. L. Malkin, B. J. Murray, A. V. Brukhno, J. Anwar and C. G. Salzmann, Proceedings of the National Academy of Sciences, 2012, 109, 1041-1045.

20 H. Washizu and K. Kikuchi, The Journal of Physical Chemistry B,

2002, 106, 11329-11342.
21 K. Kikuchi and K. Yoshioka, Biopolymers, 1973, 12, 2667-2679.
22 L. Pontoni and M. Fabbricino, Carbohydrate Research, 2012, 356, 86-92.
23 K. Kurita, T. Sannan and Y. Iwakura, Die Makromolekulare Chemie, 1977, 178, 3197-3202.
24 P. Lopes, N. Barroca, A. L. Daniel-da-Silva and B. Leite Ferreira, 2017, pp. 181-248.
25 D. J. Price and C. L. B. III, The Journal of Chemical Physics, 2004, 121, 10096-10103.
26 L. B. Wright, P. M. Rodger, S. Corni and T. R. Walsh, Journal of Chemical Theory and Computation, 2013, 9, 1616-1630.
27 Z. E. Hughes, G. Wei, K. L. M. Drew, L. Colombi Ciacchi and T. R. Walsh, Langmuir, 2017, 33, 10193-10204.
28 Q. Yuan and Y.-P. Zhao, Physical Review Letters, 2010, 104, 246101.
29 M. U. Farooq, V. Novosad, E. A. Rozhkova, H. Wali, A. Ali, A. A. Fateh, P. B. Neogi, A. Neogi and Z. Wang, Scientific Reports, 2018, 8, 2907.
30 C. G. Salzmann and B. J. Murray, Nature Materials, 2020, 19, 586-587.
31 C. Vega, E. Sanz and J. L. F. Abascal, The Journal of Chemical Physics, 2005, 122, 114507.
32 C. Vega and J. L. F. Abascal, The Journal of Chemical Physics, 2005, 123, 144504.
33 A. Pham, M. Barisik and B. Kim, The Journal of Chemical Physics, 2013, 139, 244702.
34 C. T. Nguyen, M. Barisik and B. Kim, AIP Advances, 2018, 8, 065003.
35 M. Maccarini, R. Steitz, M. Himmelhaus, J. Fick, S. Tatur, M. Wolff, M. Grunze, J. Janeček and R. R. Netz, Langmuir, 2007, 23, 598-608.
36 S. I. Mamatkulov, P. K. Khabibullaev and R. R. Netz, Langmuir, 2004, 20, 4756-4763.
37 B. Bagchi, Water in Biological and Chemical Processes: From Structure and Dynamics to Function, Cambridge University Press, Cambridge, 2013.
38 B. J. Murray, D. A. Knopf and A. K. Bertram, Nature, 2005, 434, 202-205.
39 I. M. Svishchev and P. G. Kusalik, Physical Review Letters, 1994,

73, 975-978.
40 Q. Zhu, A. R. Oganov, C. W. Glass and H. T. Stokes, Acta Crystallographica Section B, 2012, 68, 215-226.
41 V. F. Petrenko and R. W. Whitworth, Physics of Ice, Oxford University Press, Oxford, 2002.
42 W. Drost-Hansen, Science, 1969, 166, 861-861.
43 J. Lu, Y. Qiu, R. Baron and V. Molinero, Journal of Chemical Theory and Computation, 2014, 10, 4104-4120.
44 D. Nayar, M. Agarwal and C. Chakravarty, Journal of Chemical Theory and Computation, 2011, 7, 3354-3367.
45 B. Shadrack Jabes, D. Nayar, D. Dhabal, V. Molinero and C. Chakravarty, Journal of Physics: Condensed Matter, 2012, 24, 284116.
46 R. H. Henchman and S. J. Cockram, Faraday Discussions, 2013, 167, 529-550.
47 D. Nayar and C. Chakravarty, Physical Chemistry Chemical Physics, 2013, 15, 14162-14177.
48 M. Tanaka, T. Hayashi and S. Morita, Polymer Journal, 2013, 45, 701-710.
49 H. Kitano, K. Ichikawa, M. Ide, M. Fukuda and W. Mizuno, Langmuir, 2001, 17, 1889-1895.
50 K. Yamazoe, Y. Higaki, Y. Inutsuka, J. Miyawaki, Y.-T. Cui, A. Takahara and Y. Harada, Langmuir, 2017, 33, 3954-3959.
51 H. Arai, Y. Horikawa, K. Sadakane, T. Tokushima, Y. Harada, Y. Senba, H. Ohashi, Y. Takata and S. Shin, Physical Chemistry Chemical Physics, 2012, 14, 1576-1580.
52 T. Tokushima, Y. Horikawa, O. Takahashi, H. Arai, K. Sadakane, Y. Harada, Y. Takata and S. Shin, Physical Chemistry Chemical Physics, 2014, 16, 10753-10761.
53 M. Fixman, The Journal of Chemical Physics, 1962, 36, 306-310.
54 J. Wang, W. Wang, P. A. Kollman and D. A. Case, Journal of molecular graphics & modelling, 2006, 25, 247-260.
55 J. Wang, R. M. Wolf, J. W. Caldwell, P. A. Kollman and D. A. Case, Journal of Computational Chemistry, 2004, 25, 1157-1174.
56 S. Plimpton, Journal of Computational Physics, 1995, 117, 1-19.

## 4. Conclusions and future

### 4.1 Conclusions

The simulation study successfully distinguishes non-freezing and intermediate water by examining the tetrahedral order of water molecules around polymers. Furthermore, the tetrahedral order method also confirms and explains the various and complex classifications of interfacial water theories and experiments. The hydroxyl group is responsible for forming intermediate water. Meanwhile, the ether and ester groups form non-freezing water and intermediate water. Depending on high or low temperature, the ether and ester groups increase the number of non-freezing water or intermediate water, respectively. Even applying a high electric field for appearing the ice water, the water molecules still grow into non-freezing water at a distance of 1 Å to the surface of the polymer. Due to the successful classification of interfacial water by a simple method, this simulated study can reduce the cost and time for choosing biomedical materials in experiments.

### 4.2 Future

Composite materials are the development trend of the future when the properties of single materials have been studied almost fully and cannot meet the requirements for rapid development in research and practical applications nowadays. In biomedical materials areas, polymers are the primary materials for bio/blood compatibility besides 2D materials such as graphene, graphene oxide, and molybdenum oxide. Although the polymer materials used inside the human body, especially in the drug delivery area, are not easily dissolved in solvents such as water, the advanced syntheses of polymers handle neutral polymers to positively charged polymers and negatively charged polymers which are combined to form composite materials. In the future, choosing suitable polymers can be comfortable and speedy by using simulation.